SIMULATION STUDY ON TRANSFORMER REMANENCE DEMAGNETIZATION METHODS UNDER NEW ENERGY GRID-CONNECTED HARMONICS

Lappeenranta–Lahti University of Technology LUT

Bachelor’s Programme in Electrical Engineering, Bachelor's thesis

2026

Shaohan Qi

Examiner(s): A.Prof Xiaozhen Zhao

Hannu S. Kärkkäinen, D.Sc. (Tech)

ABSTRACT

Lappeenranta–Lahti University of Technology LUT

LUT School of Energy Systems

Electrical Engineering

If relevant (double and triple degrees), In co-operation with partner university/universities: Hebei University of Technology

Author's name: Shaohan Qi

Simulation Study on Transformer Remanence Demagnetization Methods Under New Energy Grid-Connected Harmonics

Bachelor’s thesis

Year of completion of the thesis:2026

57 pages, 16 figures, 3 tables and 1 appendices

Examiner(s): Professor Xiaozhen Zhao and Hannu S. Kärkkäinen, D.Sc. (Tech)

Keywords: Transformer Remanence; Demagnetization; Adaptive constant-voltage variable-frequency (CVVF); harmonic-contaminated excitation; MATLAB/Simulink

Due to the growing use of renewable-energy sources in contemporary power systems, harmonic distortion and challenging operating conditions have also increased the relevance of transformer remanence-related issues. The residual magnetism in the transformer core upon de-energization can enhance excitation inrush current, local magnetic stress, and even influence safety and stability of the power system. Hence, precise measurement of remanence and successful demagnetization is theoretically and engineering-wise important.

The present thesis aims at measuring and removal of transformer remanence in the context of renewable-energy grid-connected harmonics in the field of engineering. It first examines the hysteresis properties of ferromagnetic core materials as well as the physics of how remanence is produced. Using this, an evolution model of flux-linkage with harmonic-contaminated excitation is then discussed and the theoretical applicability of the adaptive constant-voltage variable-frequency (CVVF) demagnetization technique is elaborated based on the point of view of voltage integration and flux reconstruction. The study demonstrates that the integrated harmonic voltage elements are presented into the flux-linkage equation with coefficients inversely related to harmonic order and angular frequency, which explains why the proposed method can reduce the disturbance level theoretically.

Subsequently, a closed-loop simulation model is created in MATLAB/Simulink and SimPowerSystems. The single-phase saturable transformer model with a controlled voltage source, signal acquisition modules, and an S-function based adaptive control algorithm is

designed considering the nameplate parameters and magnetization properties of the transformer. The model represents the whole process of bidirectional saturation calibration, initial remanence calculation and exponential decay demagnetization. The simulation outcomes at various initial remanence levels indicate that the suggested approach can offer relatively high accuracy of the measurement of the remanence and lower the remanence ratio to the final residual level to a very small value. Moreover, three-phase transformer models are built to check the flexibility of the method in case of asymmetric initial remanence conditions.

In order to better represent the thesis background of harmonics in the renewable-energy grid-connected systems, an additional single-phase verification case is added by overlaying third and seventh harmonic components on the control input of the controlled voltage source, and maintaining the original model and control logic. The findings show that even though the voltage and current waveforms are increasingly distorted, the reconstructed flux-linkage trajectory remains orderly shrinking and the demagnetization process will continue to be accomplished successfully. It also supports the fact that the suggested CVVF technique would be able to withstand a particular level of robustness in the conditions of harmonic-contaminated excitation.

The paper offers a fairly full simulation and analysis model of transformer remanence measurement and demagnetization, as well as can be used to provide practical assistance in the creation of demagnetization strategies, enhancement of maintenance procedures, and operation of transformers in complex power-system conditions.

SYMBOLS AND ABBREVIATIONS

Roman characters

$e(t)$	induced voltage	V
$i(t)$	excitation current	A
R_{dc}	winding DC resistance	Ω
t	time	s
U_1	fundamental voltage amplitude	V
U_h	h^{th} harmonic voltage amplitude	V
$u(t)/\mu(t)$	applied voltage	V
a	DC voltage reference input of the S-function	V
b	measured excitation current input of the S-function	A
c	flux-linkage or integration-related feedback input of the S-function	Wb
f_n	rated frequency	Hz
I_{sat}	saturation-current threshold	A
k	exponential decay coefficient	
t_0	initial time of integration	s
$u_c(t)$	ideal control voltage generated by the CVVF controller	V
u_1	voltage command variable inside the S-function	V
u_a	phase-A voltage	V
u_b	phase-B voltage	V
u_c	phase-C voltage	V
L_a	equivalent magnetizing inductance of phase A	H
L_b	equivalent magnetizing inductance of phase B	H
L_c	equivalent magnetizing inductance of phase C	H

Greek characters

$\Phi(t)$	core flux linkage	Wb
$\Phi(0)$	initial flux linkage	Wb
$\Phi_c(t)$	flux-linkage component associated with the ideal control voltage	Wb
$\Phi(t_0)$	initial flux linkage at time t_0	Wb
φ_{sat}	saturated flux linkage	Wb
φ_{av}	average flux linkage	Wb
ω	angular frequency	rad/s
φ_0	initial remnant flux linkage	rad/s
θ_h	phase angle of the h^{th} harmonic	rad
τ	variable of integration for time	Wb
φ_a	flux linkage of phase A	Wb
φ_b	flux linkage of phase B	Wb
φ_c	flux linkage of phase C	Wb
φ_{ae}	final flux linkage of phase A after demagnetization	Wb
φ_{ae}	final flux linkage of phase B after demagnetization	Wb
φ_{ae}	final flux linkage of phase C after demagnetization	Wb
ω	fundamental angular frequency	rad/s

Subscripts

a,b,c	phases A, B, and C of the transformer

ae, be, ce	Equilibrium/final values for phases A, B, and C after demagnetization
h	harmonic order
c	control-related component
dc	direct-current or winding DC quantity
Initial	initial remanent value
th	threshold value
sat	saturation value

Abbreviations

CVVF	Constant-Voltage Variable-Frequency
DC	Direct Current
AC	Alternating Current
Pu	Per-unit system
HV	High Voltage
LV	Low Voltage
MV	Medium Voltage
S-function	user-defined Simulink control function

Table of contents

Abstract

Symbols and abbreviations

1 Introduction 1
1.1 Research background 1
1.2 Current research status 3
1.3 Main research content and structural arrangement of the paper 4
2 Theoretical basis of remanent magnetism correlation in transformers 6
2.1 Hysteresis characteristics of transformer core and mechanism of remanent magnetism generation 6
2.2 Adaptive constant voltage variable frequency remanence measurement and elimination principle 8
2.3 Theoretical analysis of the CVVF method under harmonic-contaminated demagnetization excitation 10
2.3.1 Research object and analytical idea 11
2.3.2 Voltage representation and flux-linkage derivation under harmonic-contaminated excitation 11
2.3.3 Theoretical adaptability of the CVVF method to harmonic disturbance 12
3 Simulation modeling and implementation of the single-phase transformer based on adaptive constant voltage variable frequency method 14
3.1 Configuration of simulation model for single-phase transformer 14
3.2 Analysis of single-phase simulation results 19
4 Simulation model and application of the three-phase transformer based on adaptive constant voltage variable frequency method 24
4.1 Triangular simulation model of three-phase transformer 24
4.2 Analysis of simulation results for three-phase transformer delta connection 27
5 Robustness analysis of algorithms under harmonic interference from grid-connected new energy sources 32
5.1 Analysis of the influence of harmonic-contaminated station power on the demagnetization power supply 32

5.2 Discussion on the applicability of the method under complex initial remanence conditions 35
5.3 Chapter summary 37
6 Conclusions and prospects 38
References 41

Appendices

Appendix 1. Source code of the user-defined CVVF S-function controller

DECLARATIONS

Turnitin

The originality of this thesis has been reviewed with the Turnitin similarity checking service.

AI usage

The thesis writer, Shaohan Qi, has used the following AI-tools in preparing the thesis:

1. AI tool name ChatGPT
    a. Purpose of use: Search for relevant literature and explanations of relevant definitions
    b. Explanation of the use of the tool: Search for relevant literature and explanations of relevant definitions
2. AI tool name Gemini
    a. Purpose of use: Organizing language
    b. Explanation of the use of the tool: Send the rough draft of the text or information I've already written to Gemini so it can help polish and organize it.
3. AI tool name Doubao
    a. Purpose of use: Explain the data
    b. Explanation of the use of the tool: Explaining some parameters in the literature that I didn't understand.

Responsibility

The author, Shaohan Qi, is responsible for the entire content of this thesis and has reviewed and edited the content produced as a consequence of the potential use of AI tools.

1 Introduction

The high rate of growth of renewable energy has added complicated harmonic interference to contemporary power networks with a substantial rise in the probability of transformer excitation inrush current due to remanence. Conventional techniques of demagnetization can be quite difficult to preserve accuracy under such conditions of the new grid. In this thesis, the focus is on the simulation of a new measurement and cancellation plan of transformer remanence. After examining the challenges of the harmonics that are connected to the grid, the chapter sets the research objectives, assesses the weakness of the existing technologies, and provides the overall technical background of the research.

1.1 Research background

Being the most important hub devices in the power system, power transformers form the backbone of voltage level conversion, energy distribution as well as long distance transmission. The stability of their operation is directly related to grid reliability and general quality of the power. Single-phase transformers are also commonly used in ultra-high voltage transmission lines, special power supply conditions, and massive hub substations because of their specific benefits, which include low losses, high efficiency of performance, and good capacity scalability. The transformers usually have laminated cores constructed with high-permeability crystal-oriented silicon steel sheets, and they have the usual property of ferromagnetic materials, hysteresis. The process of residual magnetic flux occurs when during maintenance work, regular power failures, or closure of no load, the magnetic domains inside the core are unable to come back to a non-magnetized state completely, and this is called core remanence.(Li et al., 2020)

The residual magnetism can cause various operational hazards. In the case of closing under no-load conditions, residual magnetism can interact with power frequency alternating magnetic fields to produce excitation surge currents as high as 6-8 rated current. Surge currents are excessive and can create extreme electrodynamic forces which continuously act on the transformer windings thus enhancing the rate at which insulation ages and causes mechanical failure. Furthermore, these currents have large DC components and higher order

harmonics, which directly cause malfunction of important relay protective devices including differential protection and overcurrent protection systems（He et al., 2018; Zhang et al., 2019). These events do not only affect usual transformer operations but can also result in bus voltage sags and harmonic pollution of the grid, which would interfere with the stability of power supply to nearby loads.

Moreover, the long-lasting residual magnetization may cause local magnetic induction intensity concentration in iron cores causing overloads in localized areas, operation noise and additional losses. The presence of these factors greatly reduces the useful life of transformers. The existing methods of managing residual magnetization in the field are based more on operational experience, so there are no standard demagnetization procedures.(General Administration of Quality Supervision, Inspection and Quarantine of the People’s Republic of China, 2010) This causes quantification of residual magnetization levels inaccuracy and inefficient control of demagnetization effectiveness, where in some instances, incomplete demagnetization is encountered or counterproductive residual magnetization effects occur as a result of over-demagnetization. In contrast to expensive field test technologies that have serious safety and parameter calibration issues, computer simulation technology has been proven to be able to precisely simulate the entire electromagnetic transient process including the generation of residual magnetization, measurement of residual magnetization, and removal of residual magnetization.(Wu, 2018; Wu, 2022) The technology also allows adjusting the parameters in a flexible way and implementing optimal demagnetization control schemes, which have a high theoretical basis and provide natural parameters instructions in the field. Thus, creation of single-phase transformer residual magnetization simulation models with the use of real equipment parameters and specific studies of the methods of eliminating residual magnetization and measuring it have significant engineering and theoretical importance.

Moreover, the engineering nature of this topic can be made even stronger by the growing use of renewable energy sources in the contemporary power systems. Photovoltaic and wind power integration with the grid at large scale usually involves the use of power electronics converters that can result in non-sinusoidal voltage and current in the network and thus worsen the harmonic related power quality issues. In such an environment, it is more important to pay more attention to transformer energization transients, residual-flux-induced inrush current, overheating, and maloperation of the protection. Hence, despite the fact that

the given study largely addresses the issue of modeling and validation of remanence measurement and elimination techniques of a single-phase transformer, the research problem is viewed in the context of the practical implementation of renewable-energy grid integration with harmonic disturbances.(Kalair et al., 2017; Eroğlu et al., 2021)

1.2 Current research status

The subject of transformer residual magnetism is an important topic which global scholars and engineers have widely researched on a variety of aspects such as theoretical mechanisms, suppression mechanisms and simulation modeling. The mature technologies in residual magnetism suppression and demagnetization technologies are mainly DC attenuation demagnetization, AC frequency conversion demagnetization, pulse demagnetization and adaptive closed-loop demagnetization.(Zhao et al., 2025; Wu et al., 2022) Of these, the adaptive constant-voltage frequency conversion approach has become the mainstay in engineering practice. It uses closed-loop control of rate of flux decay without manual changes of parameters to provide high efficiency of demagnetization, minimal residual magnetism and compatibility with different initial residual magnetism conditions.

In the meantime, recent research on the topic of renewable-energy systems has indicated that harmonic distortion has been one of the major indicators of power quality problems associated with converter-interfaced networks.(Zhao et al., 2025) The available review literature concentrates mostly on the origins, analysis and reduction of harmonics within renewable energy conversion systems, whereas articles on transformer remanence and demagnetization tend to consider energization transients, residual flux estimation and regulated switching.(Bejmert et al., 2022; Martínez-Figueroa et al., 2023) To put it differently, the research on renewable-energy harmonics and research on transformer remanence are constantly evolving; however, the direct combination of these two viewpoints remains quite restricted. It also means that there is a need to conduct basic simulation research on the elimination of transformer remanence using methods based on the engineering conditions of the integration of the renewable-energy grid.

The combination of the MATLAB/Simulink simulation toolbox and the Simscape Electrical platform has been adopted as the simulation software of choice when it comes to electromagnetic transient simulations on transformers in simulation modeling. The present

studies are mainly devoted to the simulation of excitation surge currents and hysteresis characteristic modeling but have two serious shortcomings: first, the most models use generic transformer parameters, which are not aligned well with real equipment specifications and core saturation properties and lead to the considerable difference between simulation results and field behavior. Secondly, the Powergui core simulation module does not provide detailed information about optimization logic of parameters and coordination mechanism among different modules causing difficulties in reproducibility of the models and providing limited practical recommendations to engineers.(Wu, 2018)

In order to overcome the above-mentioned constraints in the current research, this paper develops the entire process of the closed-loop remanence simulation model. The study gives thorough descriptions of how modules are built and how parameters are configured logically, which shows the implementation path of adaptive demagnetization algorithms in detail. The given strategy greatly improves the applicability of the results of the research and its practical significance, as well as effectively addresses the shortcomings in the current research on the detailed development and optimization of the parameters. The final developed simulation model has a very high level of coherence with real field working conditions and has an increased reference value.(Wang & Huang, 2019)

1.3 Main research content and structural arrangement of the paper

This research framework has been organized in the following way: Chapter 1 is the introduction that addresses the research background, discusses the possible threats of transformer residual magnetism to the safety and stability of the power system, reviews the advancement of the domestic and international research in residual magnetism measurement and removal, identifies gaps in the current research, and outlines major research content and general organization of the current paper. Chapter 2 involves a detailed theoretical study of correlation between transformer residual magnetism. First, it examines the magnetic hysteresis behavior of transformer cores in order to explain how residual magnetism can be generated, and then it develops the intrinsic relationship between residual magnetism and electromagnetic events via the magnetic flux formula $\varphi(t)=\int e(t)\mathrm{d}t+\varphi(0)$. Afterward, it describes the basic principles of adaptive constant-voltage variable-frequency residual magnetism measurement and elimination, which are well-grounded theoretically to support

the further modeling of simulations. Chapter 3 is devoted to the simulation modeling and implementation of single-phase transformers under the adaptive constant-voltage variable-frequency method, covering the main stages, i.e., parameter configuration and module development of single-phase transformer models. The analysis of the simulation results is conducted in detail, and special attention is paid to two important indicators, e.g., the greatest positive residual magnetism value and the highest negative residual magnetism value, to assess the relevance of the presented methods. Chapter 4 broadens the study to three-phase transformers by creating simulation models of the three-phase transformers using the adaptive constant-voltage variable-frequency method. Particular emphasis is placed on the modeling and realization of three-phase transformers with delta connections with careful examination of the results of simulation with regard to such characteristics as the peak residual magnetism difference in AC phases and minimum time of magnetic balance. Chapter 5 contains conclusions and perspectives, which summarizes the most significant findings and novelty of the present study, critically evaluates the current limitations, and suggests the possible research directions in the field. Lastly, the sources used in the research process are referenced to guarantee academic rigour and traceability.

It ought to also be noted that the harmonic condition of the grid connection of renewable energy is considered the engineering practice context of the issue in this thesis, and the primary research question is to confirm the validity of the suggested remanence measurement and demagnetization procedure of a single-phase transformer by simulating it.

2 Theoretical basis of remanent magnetism correlation in transformers

In order to establish a sound basis of demagnetization, this section explores the hysteresis characteristics of the transformer core and the physical process of remanence development. Rather than just basing it on mathematical derivation, the emphasis is shifted towards the electromagnetic connection between the magnetic condition of the core and its excitation history. The chapter presents the central technical reasoning of this research: the Adaptive Constant-Voltage Variable-Frequency (CVVF) technique. This involves the approach of utilizing bidirectional DC saturation to take advantage of the symmetry of the hysteresis loop to measure accurately and prepare the way in which the simulation will be implemented.

2.1 Hysteresis characteristics of transformer core and mechanism of remanent magnetism generation

Silicon steel sheets are typical ferromagnetic materials, which are used in transformer cores: the most basic electromagnetic property of them is hysteresis characteristics.(Wu, 2022) Simply speaking, the change in magnetic flux linkage within the core always follows with some delay behind a change in the excitation magnetic field outside. It can be illustrated both visually and in detail using hysteresis loops. In terms of electromagnetic induction, the flux linkage of the transformer core can be given by

$$\varphi(t) = \int e(t)\,\mathrm{d}t + \varphi(0) \tag{2.1}$$

where $\varphi(t)$ is the core flux linkage, $e(t)$ is the induced voltage, and $\varphi(0)$ is the initial flux linkage.This equation explains that the magnetic state of the transformer core is determined by the time integral of excitation process.(Li et al., 2020) Thus, the excitation current can be reduced to zero and yet the core will have a non-zero flux linkage, which is the physical cause of remanence. The external magnetic field produced by the excitation current of the transformer windings orients the directional alignment of magnetic domains in the core when alternating excitation voltage is supplied to the transformer windings. Magnetic linkage rises

slowly with increasing excitation field strength until the core achieves saturation state where the increase in magnetic linkage slows greatly. With the excitation field weakening over time, the magnetic linkage does not follow the same path back as with the field strengths but rather trails behind the changes in the field. At complete loss of excitation current, the left over magnetic domains are oriented inside the core and the resulting magnetic linkage value of those residual domains is the core remanence.

The size and polarity of residual magnetisation are not constant parameters but depend mainly on a combination of several factors such as core material characteristics, excitation voltage level and frequency, loading state before power failure and magnetic flux phase at the end of power failure.(Zhang et al., 2019) It has a high degree of irreversibility because it cannot be removed by standard no-load closure or short-term energization. In a single-phase three-winding transformer, when both high-voltage and medium-voltage sides are open-circuited, excitation signals introduced to the low-voltage side can interact directly with the core without losses. The core magnetic circuit then contains residual magnetism, which is not affected by load currents-a situation perfect to measure residual magnetism accurately and perform effective demagnetization operation.(General Administration of Quality Supervision, Inspection and Quarantine of the People's Republic of China, 2010)

In renewable-energy grid-connected systems, nonetheless, the excitation environment of transformers is not necessarily ideal sinusoidal. Due to the widespread use of a photovoltaic and wind power plant interface with the grid via power electronic converters, harmonic content can be observed in the terminal voltage and excitation current, which enhances the level of waveform distortion and power quality issues when it is operated. In these circumstances, the magnetisation path of the transformer core can deviate as compared to the case of purely fundamental frequency excitation, which complicates the development of flux linkage and the end distribution of remanent flux. Thus, the analysis of transformer remanence is needed in terms of hysteresis theory based on the engineering context of renewable-energy grid-connected harmonics.(Eroğlu et al., 2021)

$$u(\mathrm{t}) = U_1 \sin(\omega t) + \sum_{\mathrm{h}=2}^{\infty} \mathrm{U_h} \sin(\mathrm{h}\omega t + \theta_{\mathrm{h}}) \tag{2.2}$$

In case of harmonic distortion, the excitation voltage is not only the fundamental component, but a combination of many harmonic components.

$$\Phi(t) = \int u(t)\mathrm{d}t + \Phi(0) = -\frac{U_1}{\omega}\cos(\omega t) - \sum_{h=2}^{\infty}\frac{U_h}{h\omega}\cos(h\omega t+\theta_h) + \Phi(0) \quad (2.3)$$

It means that harmonic voltages will also inject more harmonic terms in the flux-linkage path, and this might make the magnetization and remanence path evolution even more difficult.(Eroğlu et al., 2021)

2.2 Adaptive constant voltage variable frequency remanence measurement and elimination principle

The adaptive constant-voltage frequency conversion technique used in the present work is fundamentally grounded on the principles of electromagnetic induction.(Wang & Huang 2019) Magnetizing branch voltage can be obtained with the help of the winding voltage and the excitation current. Then, the following equation is used to characterize the voltage acting on magnetizing inductance:

$$e(t) = \mu(t) - i(t)R_{dc} \quad (2.4)$$

where $e(t)$ is the magnetizing inductance voltage drop, $\mu(t)$ is the applied winding voltage, $i(t)$ is the excitation current, and R_{dc} is the winding resistance (Liu et al., 2021). The given equation forms the electrical foundation of the suggested approach. Real voltage that is used to power the magnetizing branch can be found through the subtraction of resistive voltage drop in the measured winding voltage, which is required to calculate the flux linkage of the core later on. Both the transformer core magnetic flux and excitation voltage have a definite integral relation. Proper control of the amplitude, polarity, and time period of excitation voltage can provide exact control of core magnetic flux. Two main steps of the methodology are remanence calibration measurement and exponential decay demagnetization. The two stages can easily be combined to form a logical closed loop system, hence they can be tightly controlled throughout the whole process.(Wu et al., 2022)

On the practical level of integrating renewable energy into the power grid, harmonic distortion can influence the measured excitation signals and the magnetic condition of the transformer core. The proposed method is derived to be applicable in such an engineering context even though harmonic injection has not been considered as a separate simulation variable in this thesis. This is why precise reconstructions of magnetizing branch voltage

and closed loop tracking of the flux linkages are especially vital since, they form the theoretical framework behind the remanence estimation and demagnetization control even with a more complicated external electromagnetic environment beyond the case of purely sinusoidal excitation.(Eroğlu et al., 2021) Hence, after the removal of the winding resistive voltage drop to the measured terminal voltage, the real magnetizing-branch voltage can also be utilized to reconstruct the flux-linkage and control the demagnetization on a closed loop.(Martínez-Figueroa et al., 2023)

In the stage of residual magnetism calibration, positive and negative excitation voltages are applied alternately to the low-voltage excitation side of the transformer.(Zhang et al., 2020) Positive DC voltage initially pushes the core magnetic flux to a positive saturation point, followed by an automatic shift to negative DC voltage that drives the flux back to the opposite saturation point.(Zhang et al., 2020) The saturated flux linkage of the transformer core can be defined in the process of bidirectional saturation as follows, depending on the symmetry of the hysteresis loop and Faraday law:

$$\varphi_{\text{sat}} = -\frac{1}{2}\int_{t_{\text{b}}}^{t_{\text{c}}} [\mu(\tau) - i(\tau)R_{\text{dc}}]\,\mathrm{d}\tau \tag{2.5}$$

where φ_{sat} represents the saturated flux linkage of the transformer core. The equation shows that the saturated flux linkage can be found by integrating the magnetizing branch voltage across the interval of positive saturation to negative saturation. The factor 1/2 is added since the outcome of the integration is related to the total flux excursion between two symmetric saturation states.During this whole process, the signal acquisition module is constantly gathering signals of the excitation voltage and current in real-time. Integrating the voltage across the magnetizing inductance, the system precisely measures the magnitude of the initial residual magnetism and thereby facilitates accurate measurement of residual magnetism and offers important reference values of future demagnetization processes. The initial remanent flux linkage may be given by

$$\varphi_0 = -\int_{t_{\text{a}}}^{t_{\text{b}}} [\mu(\tau) - i(\tau)R_{\text{dc}}]\,\mathrm{d}\tau + \varphi_{\text{sat}} \tag{2.6}$$

where φ_0 represents the initial remnant flux linkage of the transformer core. This equation helps in determining the unknown initial remanence prior to the end of the calibration process. It enables the quantitative assessment of the initial magnetic state of the transformer

core instead of the mere qualitative estimation. The main goal of the stage is to remove the effects of magnetic flux trajectories of the previous measurements by means of bidirectional saturation calibration and thus guarantee the uniqueness and accuracy of measurement readings and prevent distortions due to initial magnetic states.(Li et al. 2020; Wu et al., 2022)

When the exponential decay demagnetization stage is reached, the system works under the closed-loop control principles.(Zhang et al., 2020) Once calibration is done, the instantaneous core flux linkage can be computed in real time by

$$\varphi(t) = \int_{t_c}^{t} [\mu(\tau) - i(\tau)R_{dc}]\,d\tau - \varphi_{sat} \tag{2.7}$$

where $\varphi(t)$ is the real-time core flux linkage under the demagnetization procedure. The equation given above is a feedback variable of the closed-loop control system. If the flux linkage is continuously monitored, the controller will be able to identify the appropriate moment of voltage reversal and maintain the demagnetization process in a steady and manageable fashion. Based on measured saturation magnetic flux, it defines constant flux decay factors with cyclic changes in the polarity of the excitation voltage. Every voltage reversal represents a sequence of exponentially diminishing magnetic flux limits approaching the saturation condition, which gradually reduces the core hysteresis loop towards the origin.(Zhao et al., 2025) When this limit continues to diminish, the internal magnetic domains within the core revert to disorderly states and the remanence reduction continues until it reaches zero and stabilizes, finally eliminating all remanence. It does not involve any manual adjustment of parameters, automatically responds to different initial remanence states and guarantees a seamless, free of electromagnetic disturbance demagnetization operation of transformer models.

2.3 Theoretical analysis of the CVVF method under harmonic-contaminated demagnetization excitation

Based on the previous analysis of remanence formation and the CVVF demagnetisation principle, this section will also investigate how to do so in the presence of harmonic contamination. First, this paper will introduce the subject of the study; then, the flux-linkage expression containing harmonic voltage components will be obtained; finally, the theoretical applicability of the CVVF method to harmonic disturbance will be explained.

2.3.1 Research object and analytical idea

The penetration of inverter-based resources could also inject harmonic distortion into system voltage waveforms under renewable-energy grid-connected conditions. According to current engineering records, harmonic behavior in renewable-energy networks is strongly linked to converter properties, network impedance, and grid-connection conditions. (Australian Renewable Energy Agency, 2022) So, thinking about harmonics as a kind of engineering background makes sense when talking about transformer excitation and demagnetization issues. The current thesis has no intention of rebuilding all the harmonic magnetization history of the transformer throughout all its operation. Rather, it is aimed at addressing a more practical issue: whether the CVVF demagnetization method can still maintain a stable shrinking flux-linkage trajectory and satisfactory demagnetization performance when the demagnetization power supply or its control signal is contaminated by harmonic components.

2.3.2 Voltage representation and flux-linkage derivation under harmonic-contaminated excitation

Based on the concept of the modelling chosen in this thesis, let the hypothetical control voltage at the demagnetization step be designated as $u_c(t)$. In the case of harmonic-contaminated conditions, the real voltage delivered to the transformer winding may be expressed as a sum of the ideal control signal and other harmonic elements:

$$u(t) = u_c(t) + \sum_h U_h \sin(h\omega t + \theta_h) \tag{2.8}$$

where U_h is the amplitude of h-harmonic, θ_h is its initial phase angle and ω is the fundamental angular frequency. This expression considers the demagnetization voltage as a combination of control signal and harmonic disturbance and it is used to describe the possible non-ideal excitation that can be experienced in a renewable-energy harmonic environment. In engineering harmonic analysis, distorted voltage is generally expressed as the sum of a fundamental term and several harmonic terms.

As per the law of Faraday, and as per the flux-linkage analysis model that has already been used in this thesis, with no consideration of further high-frequency leakage-impedance effects, the core flux linkage may be expressed as

$$\Phi(t) = \Phi(t_0) + \int_{t_0}^{t} u(\tau)\mathrm{d}\tau \tag{2.9}$$

By substituting the harmonic-contaminated voltage expression into the above equation, one obtains

$$\Phi(t) = \Phi(t_0) + \int_{t_0}^{t} u_c(\tau)\mathrm{d}\tau + \sum_{h} \int_{t_0}^{t} U_h \sin(h\omega\tau+\theta_h)\,\mathrm{d}\tau \tag{2.10}$$

Denote the flux-linkage component that is associated with the ideal control voltage as $\Phi_c(t)$. Thus,

$$\Phi(t) = \Phi_c(t) + \sum_{h} \int_{t_0}^{t} U_h \sin(h\omega\tau + \theta_h)\mathrm{d}\tau \tag{2.11}$$

By integrating each harmonic term separately, the expression becomes

$$\Phi(t) = \Phi_c(t) - \sum_{h} \frac{U_h}{h\omega} \cos(h\omega t + \theta_h) + C \tag{2.12}$$

Here C is a constant of integration that may be included into the first term of the initial flux-linkage. As the result demonstrates, the coefficient of the h-th harmonic after integration is inversely proportional to $h\omega$. That is, when the harmonic amplitudes are similar, higher-order harmonics have less direct impact on the reconstructed flux linkage (Cundeva, 2008).

2.3.3 Theoretical adaptability of the CVVF method to harmonic disturbance

The CVVF method that is applied in this thesis does not use directly the local roughness of the terminal-voltage waveform to be the control variable. It rather reconstructs the electromotive force of the magnetizing branch by firstly removing the resistive voltage drop of the measured winding voltage:

$$e(t)=u(t)-i(t)R_{dc} \tag{2.13}$$

where R_{dc} is the DC winding resistance and $i(t)$ is the excitation current. Core flux-linkage feedback is subsequently derived as

$$\Phi(t) = \Phi(t_0) + \int_{t_0}^{t} [u(\tau) - i(\tau)R_{dc}]\mathrm{d}\tau \tag{2.14}$$

The control structure implies that the main feedback parameter of the CVVF algorithm has been basically based on the integral of the magnetizing-branch voltage rather than on the

roughness of the terminal-voltage waveform. Since higher-order harmonics have the factor $1/(h\omega)$ and are therefore lost due to integration, the reconstructed flux-linkage trajectory is mostly controlled by the low-frequency dominant control component even in the case where the voltage and current waveforms contain some high-frequency deformations. It explains theoretically why the algorithm can still maintain a steady decaying flux track in the presence of additional harmonic perturbation.

Moreover, CVVF demagnetization has as its main benefit the logic of closed-loop demagnetization rather than a mere observation. Equations of saturated flux linkage and of initial remanence on basis of bidirectional saturation calibration were already discussed in the earlier chapters of this thesis. Successive driving of the core with positive and negative saturation by DC excitation and finding and using the integral outcomes is an effective way of setting up a deterministic flux-linkage reference level that will be used in the next demagnetization step. The current research works on the demagnetization and remanence measurement have demonstrated that approaches depending on the state of remanence and controlled gradual decay can be used in practice as an engineering method to minimize residual flux and prevent re-energization inrush issues (Grönström, 2020; Li et al., 2025; Wei et al., 2019).

Thus, theoretically, the supplementary harmonic-injection single-phase simulation added in this thesis does not aim at reconstructing the whole harmonic operating history model. It aims to investigate if it is possible that the CVVF technique could still have an orderly shrinking flux linkage history and eventually reach effective demagnetization when a small amount of ordinary harmonic components is added to the demagnetization power supply. This analytical approach maintains the initial model and control algorithm along with developing a sensible relationship with the engineering knowledge of renewable-energy harmonic conditions (Australian Renewable Energy Agency, 2022).

As a result of the given theoretical discussion, the next single-phase simulation in this thesis incorporates typical harmonic components in the control input of the controlled voltage source in order to offer an additional validation of the flexibility of the CVVF approach in harmonic-contaminated demagnetization excitation.

3 Simulation modeling and implementation of the single-phase transformer based on adaptive constant voltage variable frequency method

As the first step in validation of the practical implementation of the CVVF strategy, the research employs a thorough single-phase transformer simulation on MATLAB/Simulink. In this chapter, the author describes how the control logic was created with the help of S-functions to perform the following two important tasks: preliminary calibration of remanence and demagnetization by exponential decay. The simulation shows how to use the excitation voltage and frequency to control the shrinking of the hysteresis loop layer-by-layer toward the origin. Various initial remanence states are examined to determine whether the method is able to decrease residual magnetism to almost zero.

3.1 Configuration of simulation model for single-phase transformer

The parameters of the nameplate of the power transformer chosen in this paper are given in Table 3.1. The saturation hysteresis curve is presented in Figure 3.1.

Figure 3.1 is the magnetic basis for the following simulation results. As shown in the graph, the transformer core has a clear nonlinear hysteresis loop. When the excitation current reaches a relatively small per-unit value, the flux linkage is no longer directly proportional to the current and starts to level off at saturation. Therefore, in the following demagnetisation simulation, the core flux linkage can be driven from the initial remanent state to the positive and negative saturation points by applying a positive and a negative excitation voltage. The two branches of the hysteresis loop also show that the flux linkage depends on the instantaneous excitation current and the prior magnetization history. Therefore, after removing or reversing the excitation, a non-zero remanent flux may still be present in the core. The proposed CVVF method is employed to perform bidirectional saturation calibration first, and then, by reversing the voltage polarity according to the flux-linkage threshold, the hysteresis loop is gradually reduced towards the origin during demagnetisation.

Table 3.1. Parameters of a single-phase power transformer

Rated frequency	50 Hz
Voltage ratio of HV/MV/LV windings(kV)	315/303.11/30
Rated capacity(MVA)	200/200/200
Rated current(A)	6666.7/659.8/634.9
Equivalent no-load loss setting in simulation(kW)	30000
No-load current percentage	15.0%

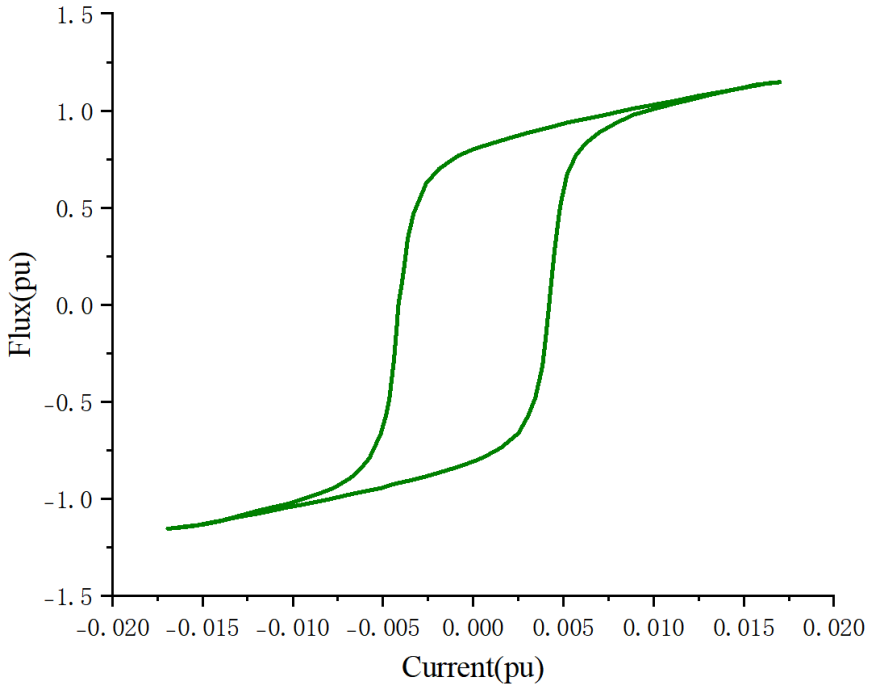

Figure 3.1. Magnetization curve of a single-phase transformer

In order to confirm the suggested approach, the saturated transformer simulation model, as presented in Figure 3.2, was created in the Matlab Simulink environment. Parameters of the model were set with the help of the single-phase transformer (Table 3.1) and real data on the saturation hysteresis curve (Figure 3.1) were determined.

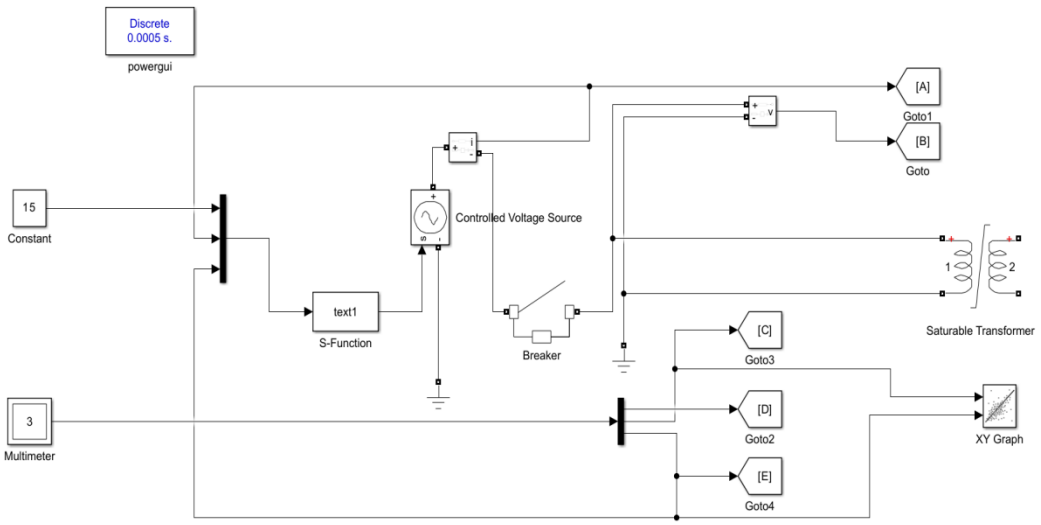

Figure3.2. Single-phase transformer simulation model

Saturable Transformer (mask) (link)

Implements a three windings saturable transformer. Click the Apply or the OK button after a change to the Units popup to confirm the conversion of parameters.

Configuration | Parameters | Advanced

Units: SI

Nominal power and frequency [Pn(VA) fn(Hz)]: [200e6 50]

Winding 1 parameters [V1(Vrms) R1(ohm) L1(H)] [30000 0.43299 0.049504]

Winding 2 parameters [V2(Vrms) R2(ohm) L2(H)] [3.0311e+05 30.696 3.5094]

Winding 3 parameters [V3(Vrms) R3(ohm) L3(H)] [3.15e+05 0.59416 0.075651]

Saturation characteristic [i1(A) phi1(V.s); i2 phi2; ...] [0 0;0 194.47;3928.4 246.33]

Core loss resistance and initial flux [Rm(ohm) phi0(V.s)] or [Rm(ohm)] [30 86]

Figure3.3. Saturable transformer parameters

The saturable transformer module, based on the Simulink library, is located in the right of the model. A double click on this module will reveal the parameter configuration interface and here the default simplified hysteresis model is disabled enabling direct use of the built-in saturation characteristic curve parameters without the need to employ external hysteresis modules. In wiring, winding 1 alone is wired to the excitation circuit, and the unconnected terminals of windings 2 are not connected to any loads or lines. The module has the functions of residual magnetism storage, saturation characteristics, excitation response and winding electrical properties. It takes an input of excitation signals by a controllable voltage source, produces equivalent excitation currents and core flux linkage and stores an initial 86Wb

residual magnetism quantity as the core platform of residual magnetism generation, measurement and elimination. Every simulation result can only be obtained with exact parameter configuration in this module.

Controlled voltage source module has a reference voltage amplitude of 15V and has the ability to change its polarity in real time. The output terminal is directly coupled in parallel with winding 1 and control input interface is coupled to the output port of the S-function block. It acts purely on control signals that are produced by the S-function algorithm, which results in automatic control of voltage polarity and output duration without human involvement. As per the instructions given by the S-function algorithm, it provides positive/negative DC voltages in the calibration steps and exponentially decaying frequency-modulated square voltages in the demagnetization steps, which supply accurate excitation signals to the transformer cores to emulate the actual demagnetization voltage excitation events. Every excitation signal is fully synchronized with the algorithmic logic so as to guarantee precision in the process of calibrating saturation in magnetic flux coupling and the gradual attenuation process.

The existing measuring module has a serial connection with transformer winding 1 to gather the excitation current signal in real time. The measurement of voltage is done across winding 1 using the measurement module that is connected in parallel to it to obtain excitation voltage signals. The integration-related feedback signal is employed as an auxiliary input to the S-function control logic, and most of the flux-linkage estimation relies on the measured voltage and current signals according to the reconstruction equation presented in Chapter 2. All the acquisition modules output terminals are uniformly connected to the S-function input through data cables allowing them to transmit signals simultaneously and without delays. It makes possible to receive critical electrical parameter (excitation current, excitation voltage, and current integral values) in real time and without distortion, which provides accurate raw data for S-function control algorithms. Such a construction guarantees the precision of residual magnetism computation, polarity identification, and demagnetization management and also works well to avoid simulation system crashes due to the signal delay or errors.

The S-function builder interface is not shown as a separate block in Figure 3.2 because it was only used to create the customised control program. After generation, the controller appears in the Simulink model as the S-function control block labeled "text1" in Figure 3.2.

A user-defined S-function control block is used in Simulink for the adaptive CVVF control algorithm. Therefore, this study adopts a customised S-function as the controller instead of a general-purpose library controller due to the state-dependent voltage reversal, saturation detection and exponential decay of the flux-linkage threshold that are required in the demagnetisation process. The three inputs to the block are the measured excitation voltage, the measured excitation current, and the integration-related signal for flux-linkage calculation. It is the output of the control command for the regulated-voltage source.

To provide a more concrete illustration of the internal contents of the S-function control block, a simplified example of the implemented MATLAB S-function logic is shown below. The S-function block in the actual Simulink model named text1 has three input signals and one output signal. The first input is the DC voltage reference amplitude; the second is the measured excitation current; and the third is the flux-linkage or integration-related feedback signal. The output of the S-function is the voltage command that drives the controlled voltage source.

The code in Appendix 1 is the MATLAB S-function program that realizes the custom CVVF demagnetisation controller in the Simulink model. It has defined a block called text1 with three inputs and one output. The first input is a DC voltage reference amplitude 'a', the second input is the measured excitation current 'b', and the third input is the flux-linkage or integration-related feedback signal 'c'. The output u_1 is the voltage command for the controlled voltage source. The current thresholds for positive and negative saturation are +3 A and -3 A in this control logic during the calibration period. After completing bidirectional saturation calibration, the controller enters an exponential-decay demagnetisation stage, and based on whether the flux-linkage threshold has been exceeded, the voltage polarity is reversed; at the same time, the threshold is reduced by a decay coefficient of 0.6 after each reversal. When the preset number of reversal cycles is reached, the output voltage will be set to zero, and thus demagnetisation will not occur.

The control program first carries out bidirectional saturation calibration inside the S-function. Apply a positive and negative DC excitation voltage alternately to reach the preset saturation-current threshold, then use the corresponding flux-linkage values to calculate the initial remanence. The program is now in the exponential decay demagnetisation phase after calibration. At this time, if the calculated flux linkage exceeds the upper or lower bound, the

direction of voltage polarity will be switched, and the threshold will be reduced by one step according to the decay coefficient. Therefore, the S-function block can perform remanence measurement and demagnetisation control in the simulation model.

Waveform observation module has a multi-module structure design with a simulation waveform observation system capable of showing real-time changes of voltage, current and magnetic flux linkage waveforms. It assesses waveform stability and the presence of transient phenomena using direct visual simulation of the whole process, which serves as an empirical proof to verify the results of the simulation.

3.2 Analysis of single-phase simulation results

According to the simulation model of Figure 3.2, the effect of various initial remanence on the efficiency of the proposed approach was investigated. It was simulated at two different initial remanence conditions, namely, maximal positive remanence and maximum negative remanence. The analysis of the simulation results is given below on the basis of maximum positive remanence result as an example.

The initial value of remanence in the saturated transformer simulation model was set to 86 Wb, and this is the upper limit for the positive remanence conditions studied here. The corresponding voltage, excitation current and flux-linkage waveforms are shown in Figure 3.4, and the change in the hysteresis loop during this process is also shown in Figure 3.5. At the beginning of the simulation, a positive DC excitation voltage is applied to the transformer core and it is driven into the positive saturation region. When the control algorithm finds that the pre-set saturation condition has been achieved, it reverses the polarity of the excitation voltage and thus directs the core flux linkage to the opposite saturation region. Both ends saturate and, as a result, provide the necessary reference data for calculating the initial remanence.

As shown in Figure 3.4, the voltage waveform changes polarity according to the control logic; thus, the excitation current is influenced by the magnetic state of the core, and the reconstructed flux linkage also changes at the same time during calibration and demagnetization. The controller has completed the calibration step and will now start exponential decay demagnetisation. At this time, the voltage polarity is frequently switched

according to the flux-linkage threshold, and thus the amplitude of the flux-linkage waveform gradually decreases to near zero in the zero-flux region. This shape of the wave is in line with the expected operating conditions of the proposed CVVF method.

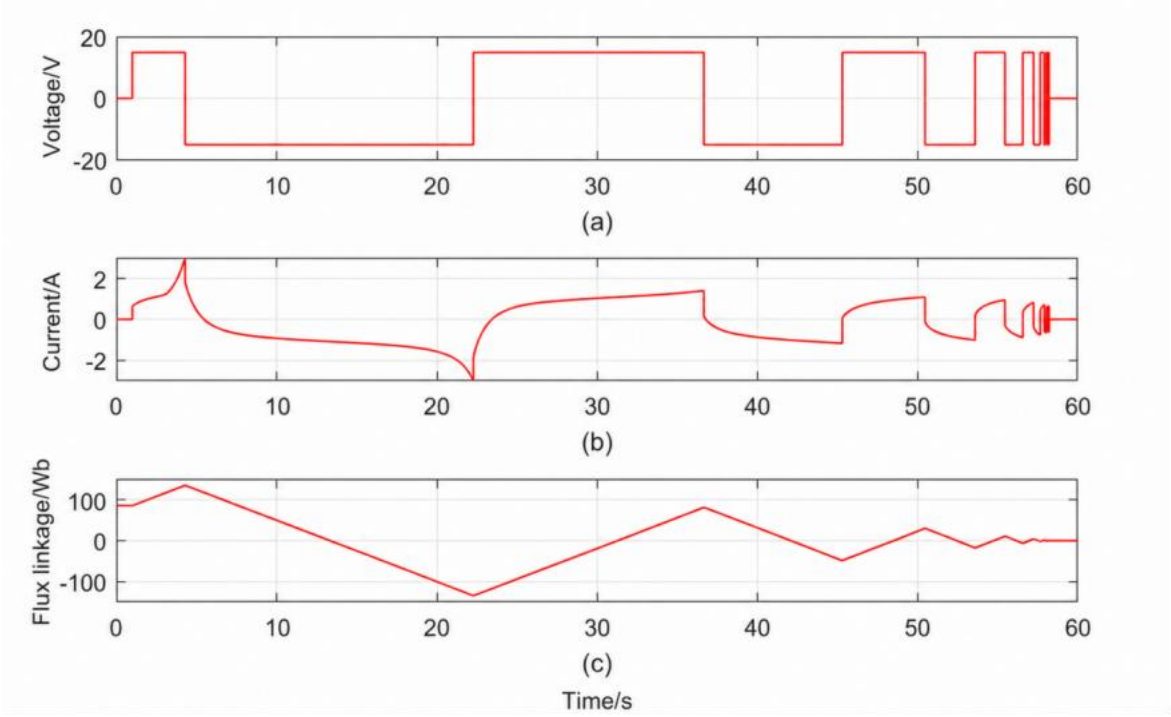

Figure 3.4. Demagnetization simulation results of a single-phase transformer (initial residual magnetism is set to the positive maximum residual magnetism point)

The exponential decay demagnetization process is subsequently carried out after the completion of the calibration process discussed above. S-function controller computes the location of core flux linkage on real time basis and changes the polarity of output voltage when the core flux linkage value surpasses the core flux linkage threshold. It can be seen in Figure 3.4(c) that in the exponential decay demagnetization process the core flux linkage exponentially decays inward with the rate of 0.6 of the threshold value defined before. This finding proves that the suggested approach can effectively remove residual magnetism in the core.

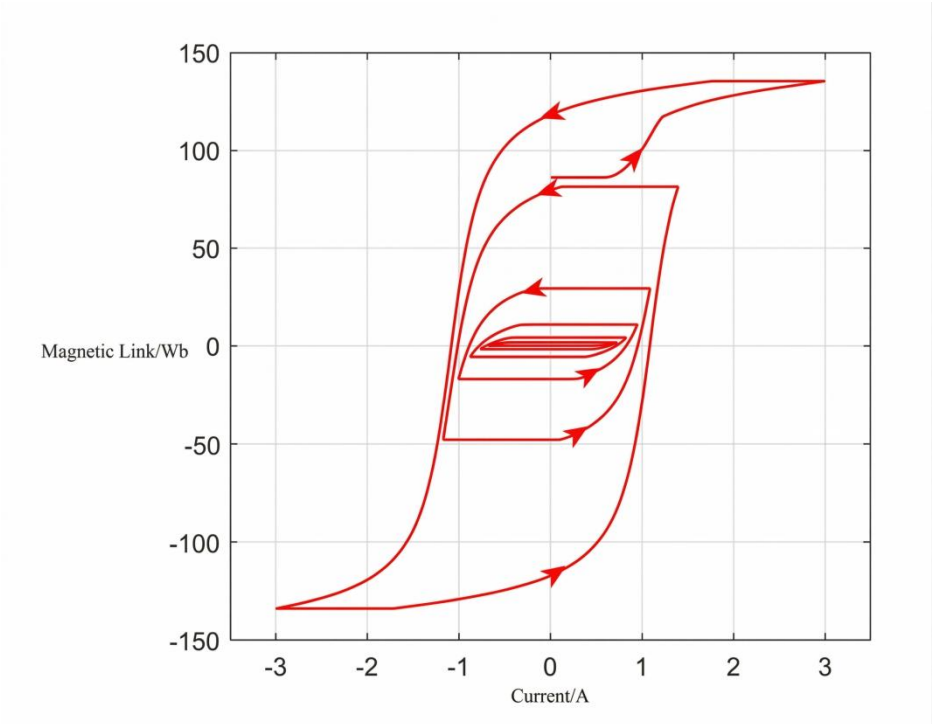

Figure 3.5. Hysteresis curve of single-phase transformer during demagnetization process

Equally so, when the initial remanence value is set to -86 Wb, that is, to the highest negative remanence point, the simulation results are depicted in Figure 3.5. The control algorithm is identical to the one in Figure 3.4. The only difference is the calibration step. Since the first thing that is applied is a positive voltage, the excitation current must be gradually increased to the preset saturation level of 3 A. The respective flux linkage should increase linearly at a rate of negative maximum remanence point up to saturation flux linkage value of 134 Wb. Thus, it takes a relatively long time until the core reaches saturation whereas the latter step is fully in line with the observations made in Figure 3.4. Hence, the suggested remanence measurement and removal procedure can dynamically change the duration between applications of the first positive voltage or, in other words, dynamically finish the calibration stage and then apply an exponential decay demagnetization stage eventually leading to a precise measurement and total removal of the remanence.

Simulations of adaptive single-phase constant voltage frequency conversion have been conducted under various initial remanence conditions and the outcomes are presented in Table 3.2. As the suggested approach can change dynamically the duration of the first positive voltage depending on the initial remanence values, the overall time of the demagnetization process changes slightly. However, the initial residual magnetism measurement of the proposed method is high with an absolute error of less than 0.5 Wb

relative to the true value, which is 0.3 percent of the knee flux linkage of the transformer. This error is largely associated with the simulation step size. With a reduced step size, the saturation flux linkage value calculated by the equation would be more precise and the measurement error would be lower, but the simulation time would be longer. At last, the simulation indicates that the residual magnetism removal results are excellent and the final percentage of residual magnetism is all less than 0.5 percent. Thus, it is clear that the correctness of the proposed method has been validated in full.

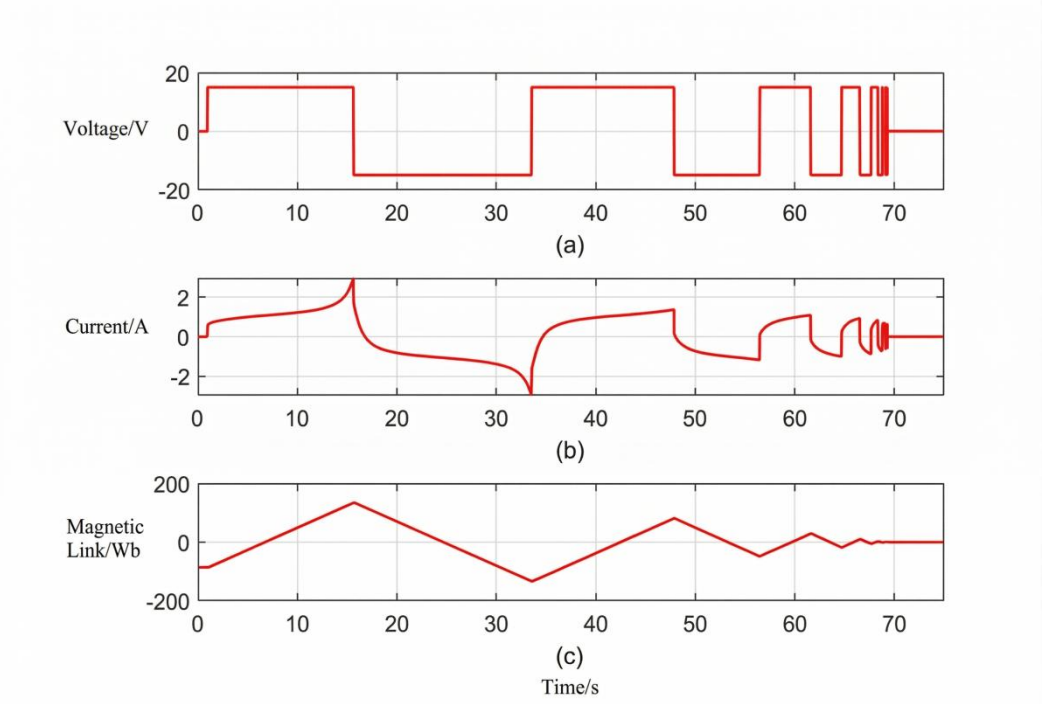

Figure 3.6. Demagnetization simulation results of a single-phase transformer (initial residual magnetism is set to the negative maximum residual magnetism point)

Table 3.2. Simulation results of single-phase CVVF method with different residual fluxes

Initial remanence，Wb	Total time，s	Remanence measurement results，Wb	Final demagnetization results，Wb	Final Remanence Percentage
86	58.2	85.5	0.51	0.31%
0	64.0	0.5	-0.002	0.0012%
-86	69.4	-86.05	0.06	0.037%

With maximum positive residual magnetism conditions, forward DC voltage initially forces the core magnetic flux to reach the forward saturation point, wherein the hysteresis loop expands towards the forward saturation end. Subsequently, reverse DC voltage drives the magnetic flux to reverse saturation point until reverse saturation point is reached, hence concluding bidirectional saturation calibration. It is observed throughout this process that the voltage application, excitation current as well as core magnetic flux waveform show coordinated variations indicating that the proposed control system is effective in establishing the desired initial calibration state. Once the calibration process has ended, the algorithm moves into an exponential decay demagnetization phase. Voltage polarity alternates regularly with a decay factor of 0.6 and the hysteresis loop recedes inwards layer by layer around the origin. Each change in voltage polarity is accompanied by a contraction of the magnetic path inward, a sign of ongoing decrease in residual flux. Figure waveforms demonstrate that there are no significant abnormal oscillations on excitation current and that core magnetic flux tends to approach the zero-flux area steadily. Such results confirm that adaptive constant-voltage variable frequency control technique is effective in suppressing the maximum positive residual magnetism allowing steady demagnetization procedures. With maximum negative residual magnetism conditions, the transformer core initially shows negative residual magnetism. The control system initially uses the predetermined excitation voltages based on pre-defined logic to bring core magnetic flux to the target saturation regions and then performs reverse calibration. The demagnetization step is then performed by successive reversal of voltage and decreasing pulse length. The same analysis of waveforms in the case of maximum positive residual magnetism also confirms that the logic of the control system for voltage application, excitation current and core magnetic flux all conforms to the expected control logic. In exponential decay, the amplitude of the magnetic flux reduces slowly over time and all the trajectories tend to converge to the origin. This implies that the suggested method is still applicable when there are conditions of maximum negative remanence.

As the simulation results show, even with an opposite polarity of the initial remanent magnetism, the adaptive constant-voltage frequency conversion technique may also provide a steady operation and effective removal of the remanent magnetism. Consequently, the suggested approach has great flexibility in response to different initial remanent magnetism states.

4 Simulation model and application of the three-phase transformer based on adaptive constant voltage variable frequency method

Expanding the research to power systems, the present chapter builds a simulation model of a three-phase transformer, concentrating on the delta-connection setup. Three-phase systems are complex because of the magnetic coupling and the possibility of extreme imbalance in remanence between the limbs. In this chapter, the CVVF method is applied to the three-phase model with emphasis on the magnetic balance effect of the centre limb. The simulation assesses the performance of the system in terms of restoring magnetic balance and under asymmetric initial remanence conditions.

4.1 Triangular simulation model of three-phase transformer

Just as with the simulation model of a single-phase transformer, to build a simulation model of a three-phase transformer it is important to start by building a simulation model based on an actual three-phase, three-limb transformer. In this research, the simulation model will be developed using a 10 kV, 50 kVA distribution transformer. The parameters detailed have been provided in table 4.1. Three phase main hysteresis curves are illustrated in Figure 4.1.

Table 4.1. Nameplate parameters of three-phase transformer

	Value
Frequency	50 Hz
Capacity	50 kVA
Voltage ratio	10 kV / 400 V
No-load current percentage	≦0.49 %
Short-circuit test impedance	1.003%
No-load loss	0.502 kW
DC resistance	High voltage side: 60 Ω; Low voltage side: 32 mΩ
Rated current	High voltage side: 2.887 A; Low voltage side: 72.1 A
Load loss	High voltage side: 0.910 kW; Low voltage side: 0.870 kW

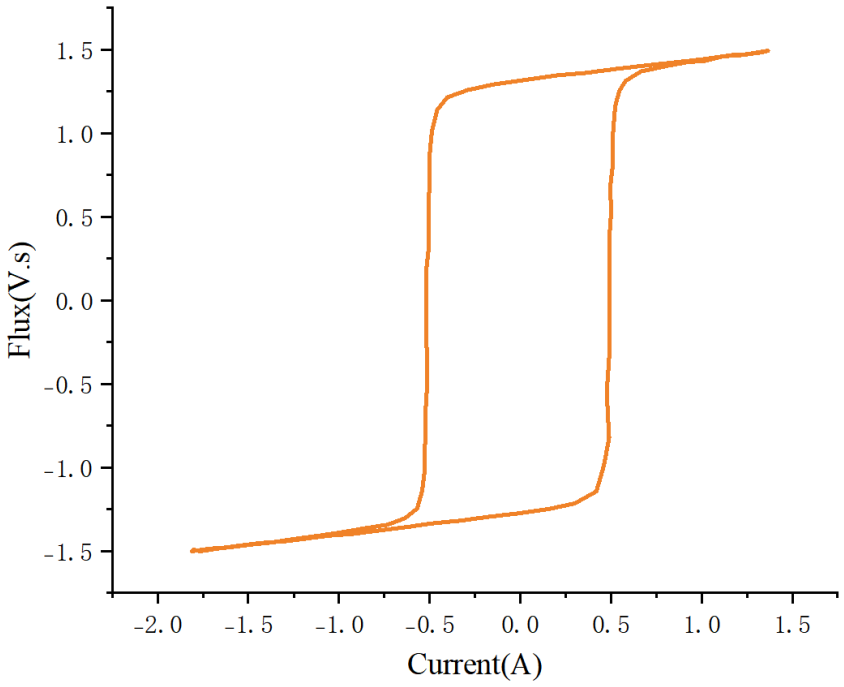

Figure 4.1. Three-phase magnetization curve

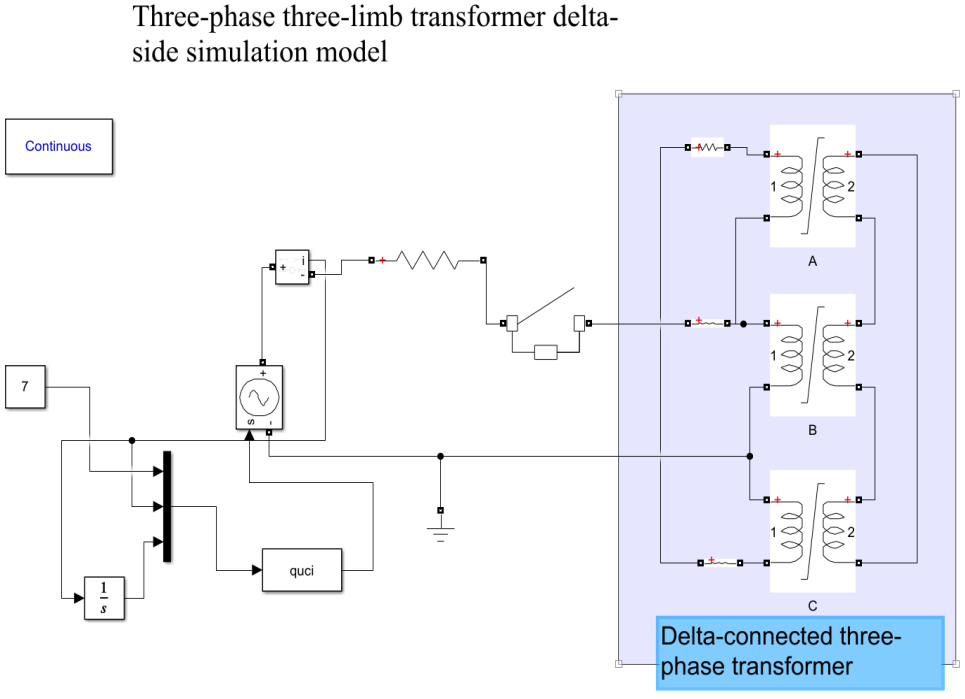

Figure 4.2. Delta-side CVVF demagnetization simulation model of the three-phase transformer

In the same manner as Section 3.2, the research develops a model of saturated transformer as illustrated in Figure 4.2 in the Matlab Simulink environment. All saturated transformer modules are internally connected to a magnetizing inductor that has a hysteresis effect. Model parameters are defined using the three-phase transformers described in Table 4.1 and the magnetizing inductor hysteresis model is selected based on the saturated hysteresis curve given in Figure 4.1. The measurement and elimination of residual magnetism of the three-phase transformer as described in this paper follows the same principle as in the case of the single-phase transformer simulation model, which is implemented by the S-function block. Figure 4.2 shows that the S-function block has three inputs i.e., the input DC voltage of the inverter of 7V, the output current and the integral value of the current. The module output is an inverter output voltage signal that is subsequently used to produce the output voltage on a controllable voltage source, which includes both the voltage output necessary to calibrate the system and the exponential decay demagnetization output. The DC reference voltage in the three-phase model is set to 7 V instead of 15 V for the single-phase model because the three-phase transformer has a different rated capacity, winding parameters and flux-linkage scale. A lower excitation voltage is selected to achieve a gentler saturation and magnetic-balancing; thus, the evolution of phase flux-linkage can be observed more clearly during calibration and demagnetisation. Therefore, this voltage value is a simulation control setting for the three-phase case and does not need to be the same as that in the single-phase model.

Figure 4.2 has the same basic control idea as the single-phase model in Chapter 3, but the transformer part has been replaced by a three-phase three-limb transformer model. Therefore, the external control structure is still composed of a DC voltage reference, an S-function-based CVVF controller, a controlled voltage source, switching elements and feedback measurement signals. The main reasons for the difference between Figure 3.2 and Figure 4.2 are that, in the case of the three-phase transformer subsystem, the three-phase windings and their magnetic coupling must be shown separately.

A controlled voltage source provides the demagnetising excitation for the selected delta-side winding in this model. The measured excitation current and the integrated flux-related signal are returned to the S-function controller. The controller will use the same bidirectional saturation calibration and exponential decay demagnetisation logic for both the single-phase and three-phase cases to set the polarity and duration of the voltage. Get the phase flux-linkage data for phases A, B and C from the internal measurement output of the three-phase

transformer, then use this data to find the magnetic balance and final remanence reduction of the three phases.

4.2 Analysis of simulation results for three-phase transformer delta connection

Based on the simulation model shown in Figure 4.2, the influence of different initial residual magnetism on the effectiveness of the proposed method is analyzed.

The verifiability of the method is made sure by the fact that the initial residual magnetism can be adjusted after the end of the calibration procedure under various three-phase initial residual magnetism conditions. Particularly, the flux linkage of the middle core column (phase B) is calibrated to a negative saturation flux linkage, whereas the flux linkage values of the two adjacent phases are calibrated to half of the positive saturation flux linkage at the same time due to the magnetic equalization process. Also, since the external voltage is applied to the phase B, the equivalent inductance of phase B will be saturated earlier than the inductances of the other two phases A and C. Hence, the amount of current flowing through inductor may be approximated as the inverter output current. Hence, the performance of phase B in the calibration process is the same as the direct interaction of the voltage with a single-phase transformer. The simulation validation of the three-phase transformer constant voltage frequency conversion method is aimed at examining the calibration impact of the flux linkages of phases A and C, namely, the impact of the magnetic equalization phenomenon leading the flux linkages of phases A and C to adjust to equal. Also, in order to check the effect of the transformer connection method, simulation verification needs to be done on the delta side. The simulation testing will be done at two levels: (1) the initial residual magnetism of phase A and phase C has the largest difference; (2) the largest positive residual magnetism of phase B leads to the shortest duration of magnetic balance (since the magnetic balance process takes place at the same time as the calibration of phase B).

① Maximum remanence difference between AC phases

In the following analysis, φ_a, φ_b, and φ_c refer to the phase flux linkages of phases A, B, and C respectively, and u_a, u_b, and u_c are the corresponding phase voltages in the following analysis. L_a, L_b and L_c are the equivalent magnetizing inductances of phases A, B and C,

respectively. Initiate the initial remanence of L_a, L_b, and L_c with 0 Wb, 0.4 Wb and -0.4 Wb respectively. This places the A and C phases at the positive and negative remanence maximum point respectively, indicating that the maximum difference in initial remanence has been set. The results of the simulations are illustrated in Figure 4.3. Phase B has a positive square wave voltage of 7V imposed on it at 0.1s, φ_b starts to rise in Figure 4.4 until it reaches positive saturation. The value of u_a is lower than u_c in the initial state following the application of voltage in Figure 4.2. It is so because the hysteresis model is imperfect, and the hysteresis curve must rapidly approach one branch of the main hysteresis curve (in this case, the descending one). Nevertheless, even with such a defect in the hysteresis model, the path of the hysteresis curve also fulfils the physical properties of a first-order inversion curve. Hence, typically, in the initial positive voltage interval, since inductor L_a saturates less than L_c (negative saturation) and therefore inductance $L_a$is higher than that of L_c, the value of u_a is larger than that of u_c, which finally reduces the difference between φ_a and φ_c significantly.

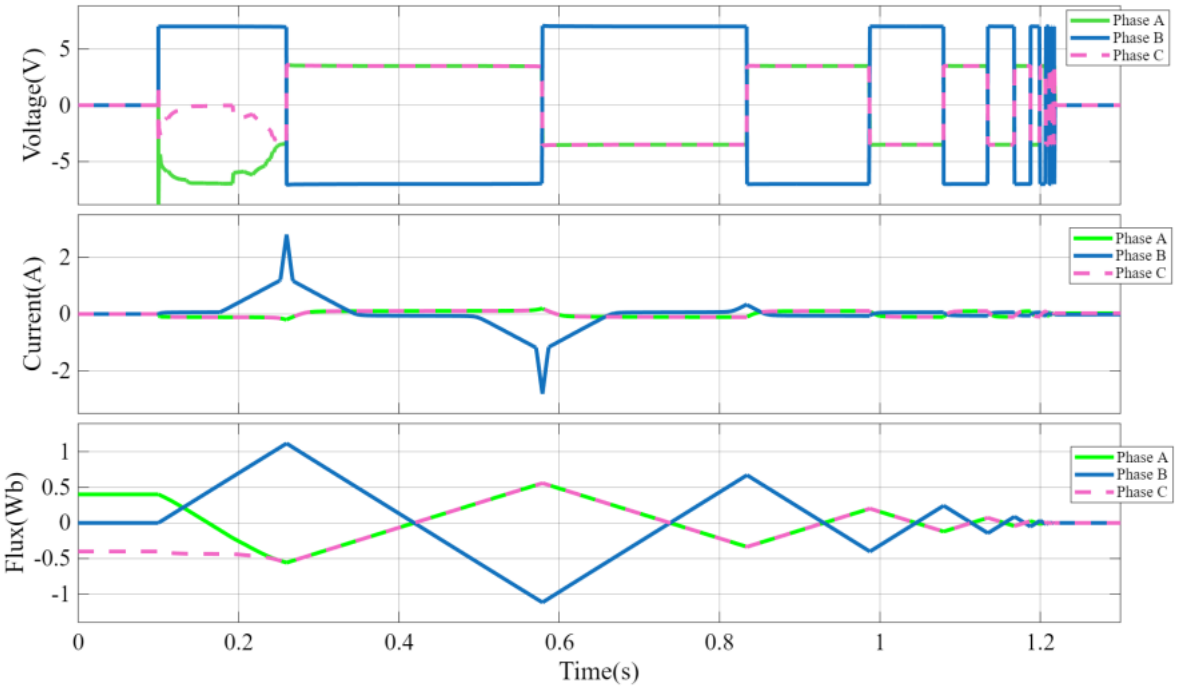

Figure 4.3. Simulation results of three-phase transformer demagnetization under the maximum remanence difference between phases A and C

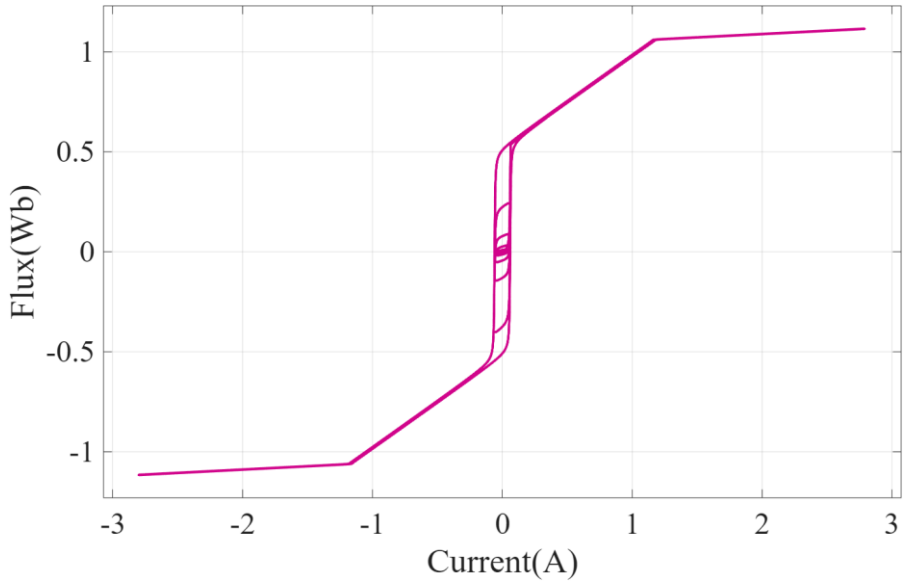

Figure 4.4. Changes in the hysteresis curve of phase B during demagnetization

Upon achieving the saturation current of 3A, the output current, the controller changes the polarity of the output voltage to negative. Following this, φ_b reduces whereas φ_a and φ_c rise as shown by the trajectory branches in Figure 4.4. In Figure 4.4, as the output current has a negative saturation current of -3A, there is almost no distinction between φ_a and φ_c, which are both half of the saturation flux linkage, and φ_b is negative saturation flux linkage of -1.14 Wb. It should be noted that in Figure 4.3, the current in is significantly higher than the current in L_a and L_c, which means that the current in the inductor L_b can be approximated as the inverter output current, which agrees with the analysis made earlier in the current section.

Following the completion of the calibration procedure mentioned above, the exponential decay demagnetization procedure is carried out. The S-function controller computes the location of the core flux linkage at real time and upon exceedance of the flux linkage value over the flux linkage threshold, it changes the output voltage polarity. As can be seen in Figure 4.4, in the course of the exponential decay demagnetization process, the core flux linkage decreases exponentially inward by 0.6 times with a pre-defined threshold used as the limit. In order to measure the ultimate outcome of the demagnetization, an average flux linkage φ_{av} is introduced and determined by the following equation:

$$\varphi_{av} = (|\varphi_{ae}| + |\varphi_{be}| + |\varphi_{ce}|) / 3 \quad (4.1)$$

In this case φ_{ae}, φ_{be}, and φ_{ce} are the values of the flux-linkage associated with the three-phase inductances after demagnetization.

This means that the last average flux linkage φ_{av} is 0.0052 Wb, which is just 0.5 percent of the knee-point flux linkage value. Moreover, the original remanence of the three phases, computed values are 0.3929 Wb, 0 Wb and -0.3929 Wb respectively. The largest discrepancy between them and the remanence set initially in this simulation is 0.0071 Wb, which is only 0.68 times the knee-point flux linkage value. This outcome indicates that the suggested approach is able to precisely quantify and eliminate core remanence even in the case where the AC phases have the largest difference in remanence.

② Shortest duration of magnetic equalization

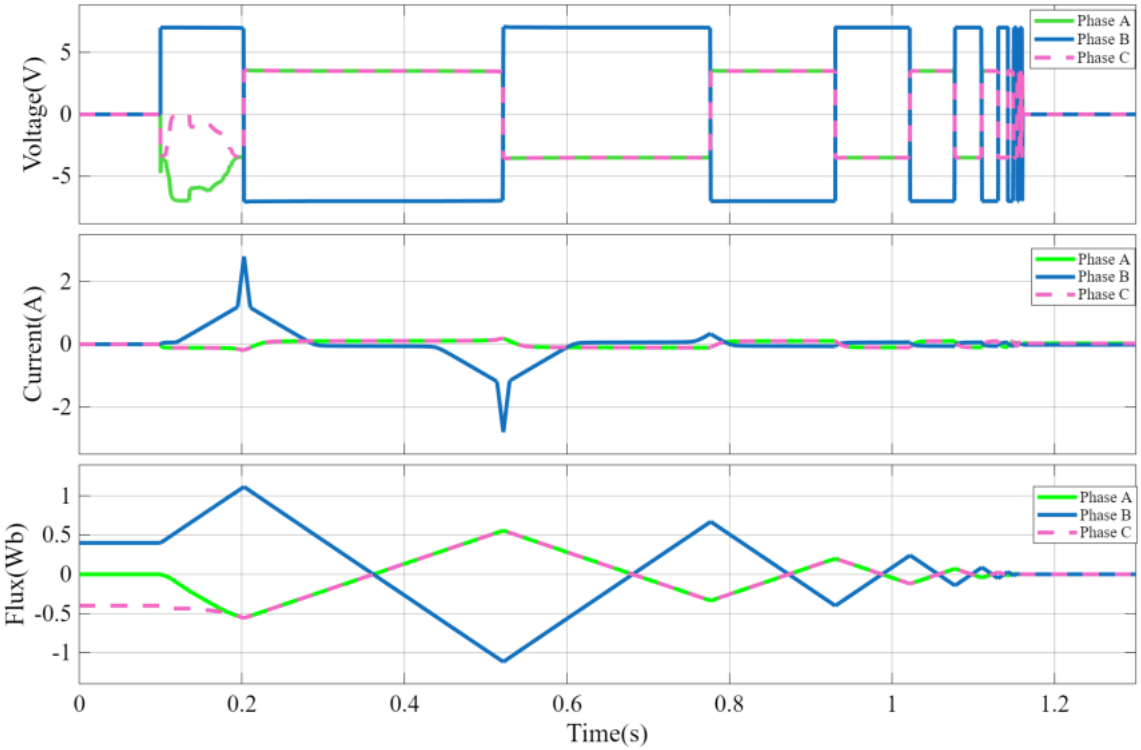

Figure 4.5. Demagnetization simulation results of a three-phase transformer (shortest duration of magnetic equalization)

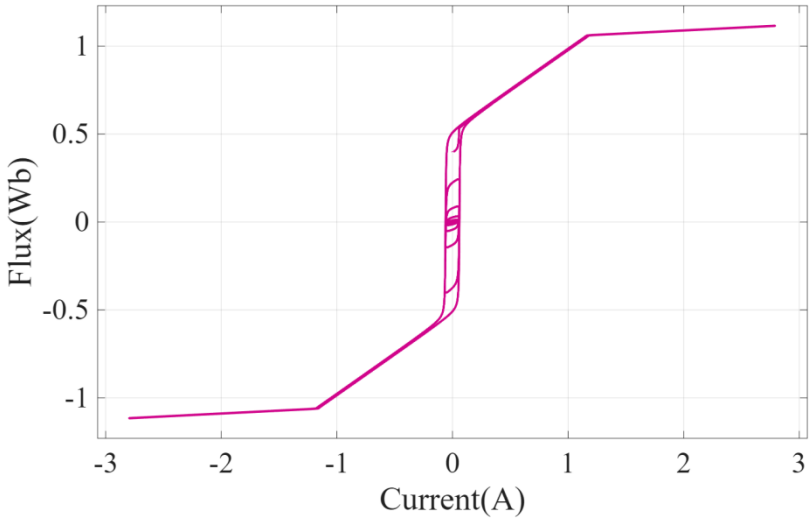

Figure 4.6. The changes in the hysteresis curve of phase B during the process of demagnetization (shortest period of magnetic equilibrium)

Since the magnetic equalization phenomenon happens at the same time as the calibration process of phase B, the minimal duration of both the calibration process and the magnetic equalization is achieved by setting phase B to the highest positive remanent value of 0.4 Wb. The initial remanence values of L_a and L_c are set to 0 Wb and -0.4 Wb, respectively. All the other configurations of the simulation model are identical to those of (1) simulation and the simulation results are given in Figure 4.5. The calibration process is finished as soon as the S-function controller identifies that the output current has saturated at time 0.53 s. It can be seen in Figure 4.6 that even though the time of the magnetic equalization effect is very small, it is capable of achieving equality between the AC phase fluxes at the end of the calibration process, thereby eliminating the effects of the initial remanence distribution and achieving successful calibration of the initial remanence of the three phases. Then again, the flux of three phases decays toward minimum value at an exponential rate of 0.6, finishing the remanence elimination operation. The last average flux φ_{av} is 0.0051 Wb, or merely 0.5 percent of the knee flux amount. The calculated values are the following: 0.4 Wb, -0.0074 Wb, and -0.3926 Wb. The maximum measurement error of the initial residual magnetism set in this simulation is 0.0074 Wb, which is just 0.71 percent of the knee-point flux linkage. The result indicates that the suggested approach is able to correctly measure and cancel out the residual magnetism of the iron cores provided that the magnetic equilibrium period is the least possible.

5 Robustness analysis of algorithms under harmonic interference from grid-connected new energy sources

The preceding chapters have confirmed that the proposed CVVF remanence measurement and demagnetisation method works properly in a standard single-phase and three-phase simulation environment. However, the operating conditions of transformers in the practical environment of renewable-energy grid connection are generally more complex. The demagnetisation power supply may be distorted by harmonic distortion, and the initial distribution of remanence in field transformers is also asymmetric or difficult to determine. Therefore, this chapter will explore the robustness and engineering applicability of the proposed method in non-ideal environments further. Analysis of harmonic-contaminated demagnetization excitation and complex initial remanence conditions, followed by a short chapter summary.

5.1 Analysis of the influence of harmonic-contaminated station power on the demagnetization power supply

Engineering practice requires that external demagnetization devices typically require connection to the station service AC supply of substations or renewable-energy stations. If the system side has a significantly large number of grid-connected photovoltaic or wind-power devices, the voltage waveform can be contaminated by some level of harmonics, which can also impact the power quality of the demagnetization device. In such environments, the demagnetization excitation signal might not be as smooth as it should be, rather there will be local distortion and high-frequency disturbance that will directly influence both voltage and current response during the demagnetization period.

To capture the "renewable-energy grid-connected harmonics" setting of the thesis title at the simulation stage, another comparative case was included into the single-phase model in Chapter 3. Here, all the initial saturable transformer module, signal acquisition modules and S-function control logic remained intact, and extra harmonic elements were added to the control voltage of the controlled voltage source to recreate the condition of operation where the demagnetization power source is polluted with harmonics. Precisely, they are the 3rd-

order and 7th-order harmonic components incorporated to produce a representative non-ideal excitation condition (Figure 5.1). In this additional case, the harmonic components are added to the control input of the controlled voltage source. The injected signal is composed of the original CVVF control signal plus 3rd- and 7th-order sinusoidal components with selected amplitudes only to create a representative distorted excitation condition, rather than to model the entire converter harmonic spectrum.

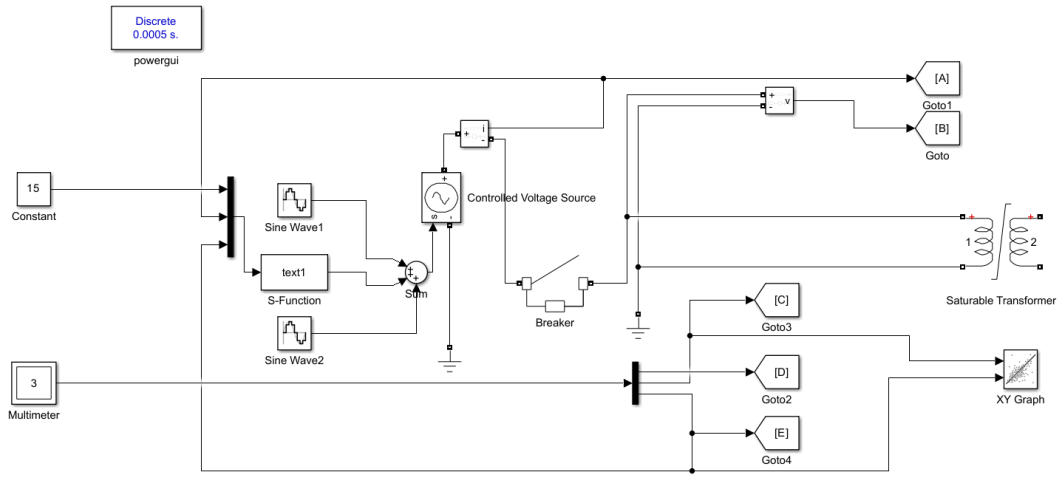

Figure 5.1. Modified single-phase CVVF demagnetization simulation model with 3rd- and 7th-order harmonic injection

The supplementary simulation findings indicate that when the 3rd-order and 7th-order harmonics were introduced, the terminal voltage and excitation current signals were seen to be much more fluctuating and locally distorted in comparison with the baseline case, as shown in Figure 5.2. The initial smooth waveforms displayed high-frequency oscillatory properties during certain time intervals, which is indicative of the fact that the demagnetization excitation had gone out of the ideal state, and it was near to the possible engineering practice in real life that can happen in the renewable-energy grid-connected environment.

Nonetheless, the overall demagnetization process was neither out of control due to harmonic interference. As demonstrated by the simulation, the flux-linkage trajectory also continued to follow a somewhat well-defined shrinking pattern towards the center, and the hysteresis loop at the exponential decay phase was also able to slowly shift towards the origin (Figure 5.3). This means that the introduced harmonics essentially altered the behavior of the voltage

and current waveforms did not effectively alter the dominant demagnetization path of the suggested approach.

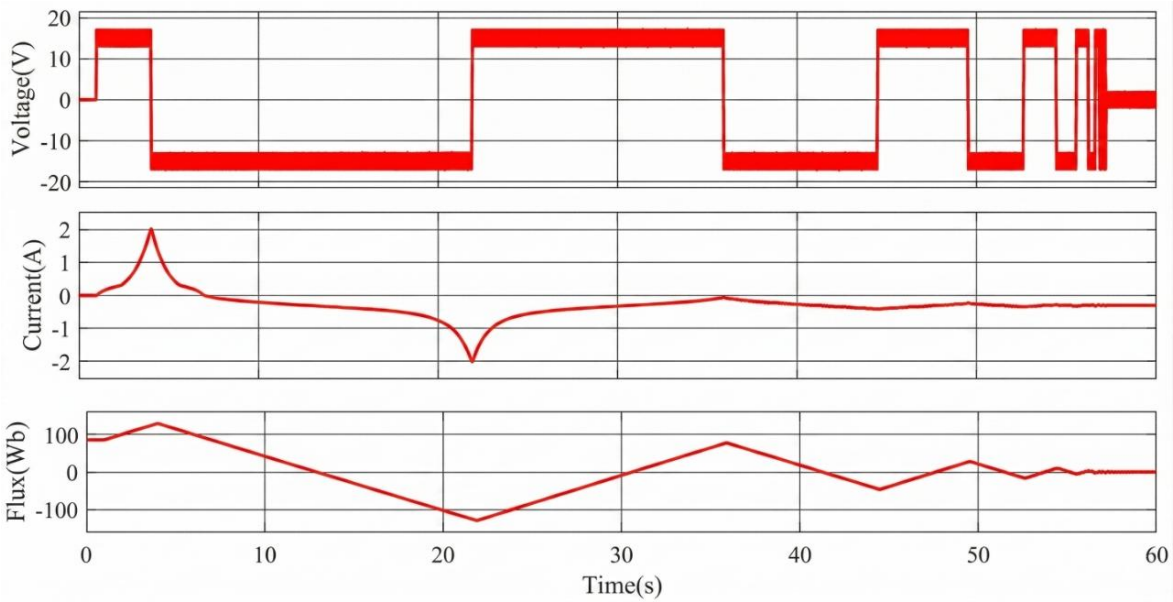

Figure 5.2. Simulation results of single-phase CVVF demagnetization after injection of 3rd and 7th harmonics

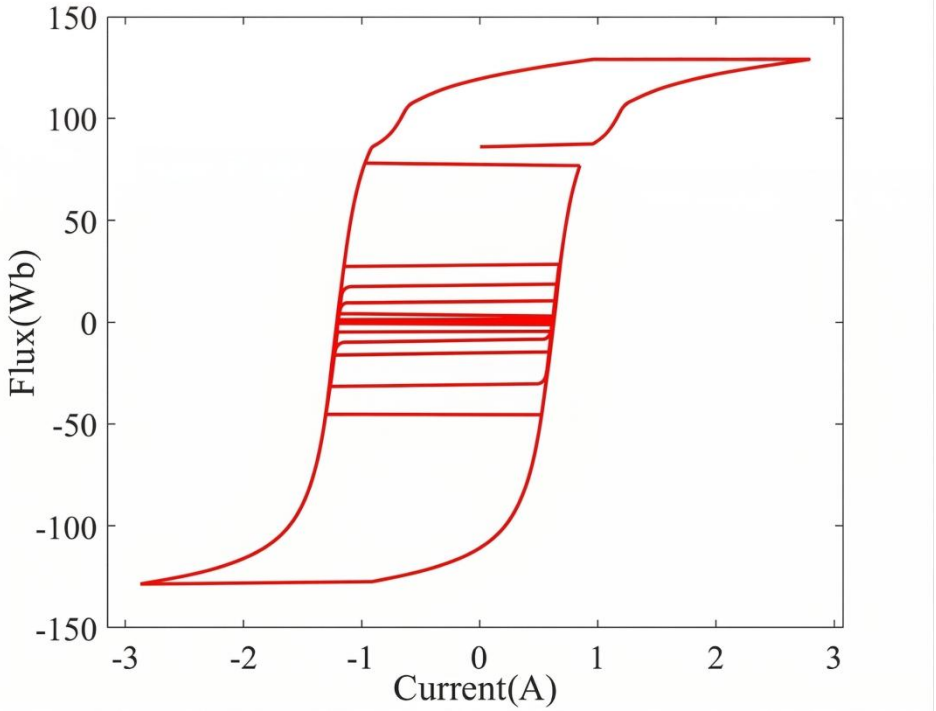

Figure 5.3. Hysteresis loop during demagnetization of a single-phase CVVF after injection of 3rd and 7th harmonics

Further, based on the control-process viewpoint, the S-function block was also capable of finishing threshold detection and voltage polarity reversal as per the flux-linkage feedback which suggested that the initial closed-loop control logic would have worked well even with harmonic-contaminated excitation. It could then be inferred that the suggested CVVF approach is still adaptable and stable in case demagnetization excitation is contaminated by a particular level of harmonics. The outcome promotes the engineering importance of this work and demonstrates that the technique is not fully dependent on the perfect and absolutely pure power-supply conditions, but can be used even in the cases when some waveform distortion may be present in reality.

5.2 Discussion on the applicability of the method under complex initial remanence conditions

Other than the fact that the demagnetization power supply can be contaminated by harmonics, the initial remanence condition of field transformers after actual operation is generally more complicated than in the ideal simulation environment. Other factors, including but not limited to the moment of de-energization, operational history, load fluctuations, and prior magnetized status, have the potential to put the transformer into the demagnetization mode with a relatively non-uniform initial magnetization. This complexity can also manifest itself as an imbalance between the remanence distributions of the three phases of three-phase transformers, thus making it harder to control demagnetization.

In this section an extremely asymmetrical and non-standard set of initial remanence conditions are established in the three-phase transformer model by setting the maximum phase-to-phase difference to higher than 0.55 Wb (i.e., φ_a= 0.45 Wb, φ_b= -0.35 Wb, φ_c= -0.10 Wb with phase A approaching the unidirectional deep saturation limit).

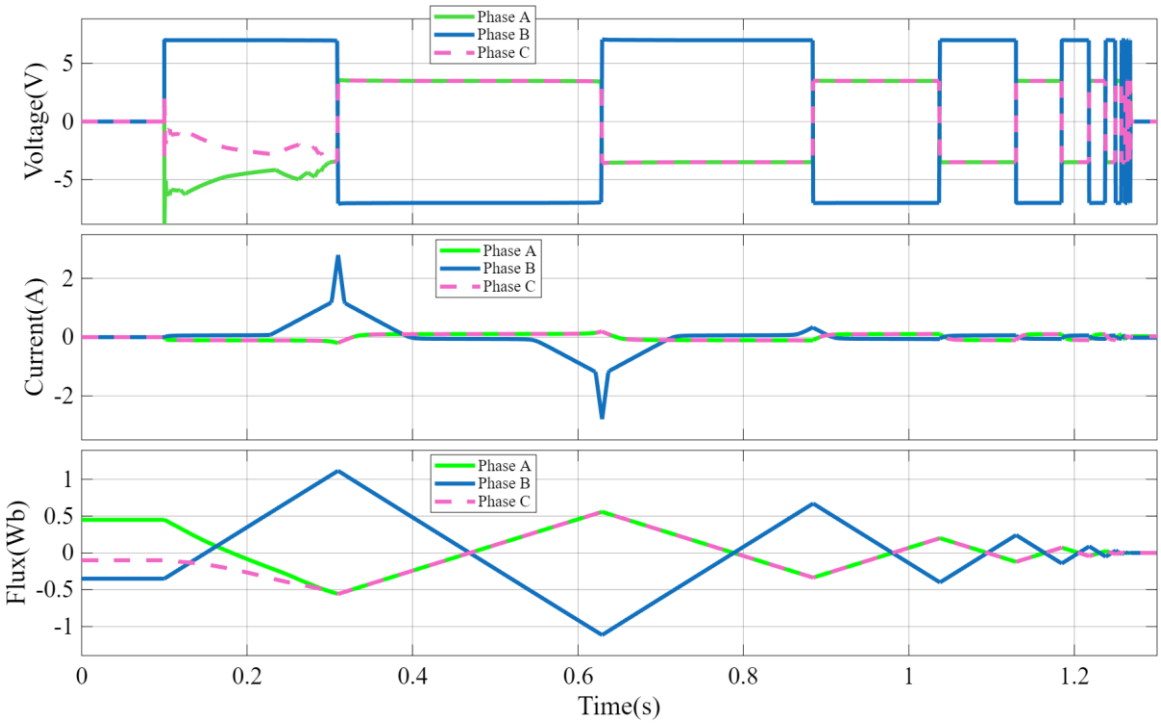

Figure 5.4. Three-phase demagnetization waveform under highly asymmetrical initial remanence conditions

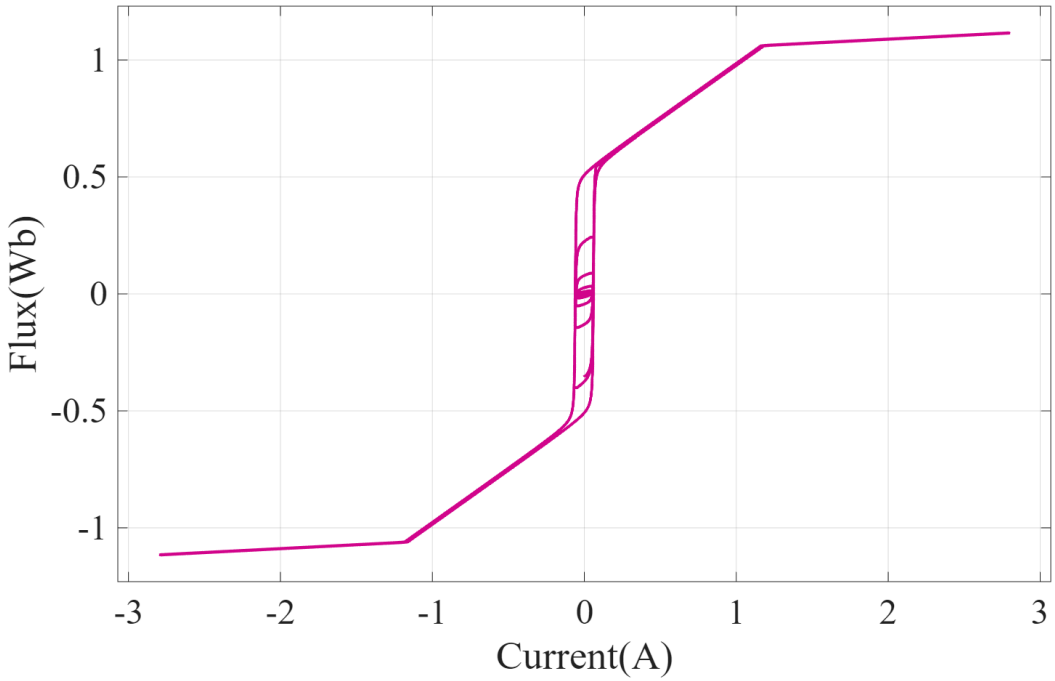

Figure 5.5. Hysteresis trajectory of phase B under highly asymmetric initial remanence conditions

With the comparation between the three-phase simulation results provided in Chapter 4 and Figure 5.4 and Figure 5.5, in the case of initial unbalanced magnetic conditions, the proposed

approach will eventually lead the system to a low remanence level using bidirectional saturation calibration and the resultant exponential decay process. It implies that the method does not entirely depend on idealized and symmetrical initial-state settings, but has some level of adjustability. Put differently, the primary control mechanism of the method may still work well even when the initial magnetic condition is somewhat complicated.

The engineering standpoint is that this characteristic can be applied to practice. The starting state of remanence of field transformers is not generally easy to forecast with accuracy ahead of time. When a demagnetizing technique is overly sensitive to the starting condition, it will inevitably have a low engineering application value. By way of contrast, the given CVVF approach begins by setting a recognizable saturation reference limit and subsequently performs the remaining steps of the demagnetization procedure, which, to a certain degree, decreases the effect of complicated initial magnetic conditions on the end demagnetization outcome. Thus, the approach does not only fit the standard simulation conditions but has the capability to be expanded into more complicated field contexts.

5.3 Chapter summary

The analysis of this chapter also focused on the strength of the suggested adaptive constant-voltage variable-frequency (CVVF) demagnetization approach due to the presence of harmonics in the grid-connected renewable-energy system. It was found that upon incorporation of the 3rd-order and 7th-order harmonic components into the demagnetization excitation, even though the distortion of the voltage and current waveforms increased, the total demagnetization process continued to be stable, and the flux-linkage trajectory and the hysteresis loop still slowly approached the origin. At the same time, with the consideration of complex initial remanence conditions in the three-phase model, it is clear that the suggested method also has some flexibility in dealing with non-regular initial magnetic conditions. Hence, the developed method may be used not only in the baseline simulation conditions but also possesses some engineering application potential.

6 Conclusions and prospects

The present thesis builds an integrated simulated environment that will be used to take accurate measurements of remanence and efficient demagnetization of transformers in the MATLAB/Simulink and SimPowerSystems simulation environment. The research includes all stages of the research chain: the physical process of transformer remanence, the application of adaptive constant-voltage variable-frequency (CVVF) demagnetization strategy, model structure, parameter alignment, stability control of simulation, and additional case checking. Based on these considerations, a fairly comprehensive and replicable simulation system on the analysis of transformer remanence and demagnetization studies has been created.

Initially, theoretically, this thesis describes the mechanism of transformer remanence formation using the hysteresis properties of ferromagnetic core material as well as the integral relation of flux-linkage. Besides, the analysis is widened by the introduction of harmonic-contaminated excitation expressions and the derivation of the corresponding flux-linkage development process. It is shown that harmonic voltage components are introduced into the flux-linkage equation when integrated with coefficients that are inversely proportional to the harmonic order and angular frequency. It gives a theoretical justification of why the flux-linkage feedback that is employed in the CVVF approach is more insensitive to high-frequency disturbances compared to voltage waveform itself. Thus, the thesis does not just develop a simulation model but also add to the physical explanation of the disturbance attenuation performance of the suggested method.

Second, with regard to model construction, it is possible to make the entire system operate in a coordinated way through the interaction of the most important modules such as the saturable transformer block, the controlled voltage source, the signal acquisition links, the control logic based on the S-function, and the Powergui discretization environment, so that the whole system is able to conduct the closed-loop remanence measurement and demagnetization process in a consistent and reliable fashion. As the simulation findings suggest, the chosen parameter arrangement is efficient in the sense that it can be used to represent the real behavior of transformer excitation and saturation behavior. Specifically, the step-size of 0.0005 s offers a good trade-off between numerical stability, computational

cost, and transient-response precision, which is necessary to ensure convergence and maintain the credibility of the simulation outcomes.

Third, the simulation outcomes of single-phase are validated to prove that the CVVF approach suggested can be used to measure remanence with high accuracy and can also be used to effectively demagnetize under various initial remanence conditions. The comparison between various initial states reveals that the method will dynamically change the calibration and demagnetization process depending on the magnetic state of the core. The measured remanence error is still insignificant and the ultimate residual remanence ratio decreases to an extremely low value. The findings support the validity of the bidirectional saturation calibration plan and the efficiency of the exponential decay demagnetization law.

Finally, a new harmonic-injection scenario is developed starting with the initial single-phase model by adding both 3rd and 7th order harmonic elements to the control input of the controlled voltage source and preserving the original transformer model, signal acquisition structure, and S-function control logic. This additional verification does not recreate the entire operating history of the transformer in harmonic conditions; rather, it is concerned with whether the proposed demagnetization strategy will still be viable when the demagnetization excitation is polluted with harmonics. As indicated by the findings, even though the voltage and current waveforms are more distorted, the trajectory of the flux linkage remains orderly decreasing and the demagnetization can still be done successfully. This result also confirms the theoretical consideration that the CVVF approach possesses some level of robustness in presence of harmonic-contaminated excitation environment.

Altogether, the current work deals with the modeling, measurement, theoretical explanation and demagnetization approach of transformer remanence, but not with the systematical parametric comparison of various harmonic spectra, harmonic amplitudes or converter operating modes of renewable-energy systems. Hence, the term the new energy grid-connected harmonics in the thesis title can be taken as the engineering application context and the practical incentive behind the research whereas the main contribution of this thesis is the creation and validation of a remanence-centered simulation and demagnetization framework in that context. In this regard, the research enhances the applicability of earlier studies by decreasing the parameter ambiguity, elucidating the implementation logic and enhancing the link between the theoretical analysis and simulation confirmation.

However, despite the above, this paper has a number of limitations. The harmonic background is presented in the thesis mostly due to theoretical consideration and additional excitation perturbation validation, but not as part of a complete comparative study that incorporates various harmonic spectra and operating conditions. Also, the current work is not yet experimentally verified and measured in hardware. However, the future work should be extended into a minimum of three directions, which are the following: firstly, integrating more realistic converter-generated harmonic sources into the framework of transformer simulation to investigate how they affect the accuracy of remanence estimation, demagnetization performance and energization transient response; secondly, conducting more systematic sensitivity analysis on the parameters like harmonic amplitude, harmonic order, and decay coefficient; and thirdly, integrating simulation with scaled experimental platforms or measurement systems to enhance the engineering credibility of the proposed method even further.

Summing it up, the present thesis offers a practical simulation model of measuring transformer remanence and demagnetization along with an additional theory and simulation-driven interpretation of its flexibility within harmonic-related engineering context. The findings show that the suggested approach is theoretically important and practically useful in the field of transformer maintenance, demagnetization strategy development, and the enhancement of functional reliability in a complex power-system environment.

References

Bejmert, D., Kereit, M. and Boehme, K., 2022. Controlled energization procedures of power transformers. International Journal of Electrical Power & Energy Systems, 135, 107555. Available at: https://doi.org/10.1016/j.ijepes.2021.107555

C. Wei., W. Xu., X. Zhang., X. Li., Y. Liu., Y. Wang., and Z. Yan., 2019. Novel Remanence Determination of Power Transformers with the Help of Measured Magnetizing Inductance, Energies, 12(24), 4616. Accessible at: https://www.mdpi.com/1996-1073/12/24/4616 (visited on 13 April 2026).

Chen, H. (2017) Steady-state analysis of power systems. 4th edn. Beijing: China Electric Power Press.

Cundeva, S., 2008. A transformer model on the basis of the Jiles-Atherton theory of ferromagnetic hysteresis, Serbian Journal of Electrical Engineering, 5(1), pp. 21–30. Available at: https://files01.core.ac.uk/download/pdf/26094878.pdf (Accessed: 13 April 2026).

Dong, Z., Li, D., Zhang, Z., Yang, Y., Zhou, J., He, W., Pei, X., Gao, J., Chen, S. and Pan, Z., 2025. Research on the Remanence Measurement Method of Transformers Based on the Degaussing Hysteresis Loop, Applied Sciences, 15(10) p. 5375. Accessed in: <https://www.mdpi.com/2076-3417/15/10/5375> (Accessed on 13 April 2026).

Eroğlu, H., Cuce, E., Cuce, P.M., Gul, F. and Iskenderoğlu, A., 2021. Harmonic problems in renewable and sustainable energy systems: A comprehensive review. Sustainable Energy Technologies and Assessments, 48, 101566. Available at: https://doi.org/10.1016/j.seta.2021.101566

General Administration of Quality Supervision, Inspection and Quarantine of the People's Republic of China (2010) Operating procedures for power transformers: DL/T 572–2010. Beijing: China Electric Power Press.

Grönström, N., 2020. Optimal demagnetization of transformer after winding resistance test. Available on: https://www.diva-portal.org/smash/get/diva2:1537658/FULLTEXT01.pdf (Accessed: 13 April 2026).

Guo, Z., Wei, J., Zhao, X., Yang, D., Zhang, S. & Li, K. (2025) Research on elimination method of residual magnetism in large power transformers based on energy storage oscillation. *Proceedings of the CSEE*, 45(24), pp. 9796–9807

Harmonic Study - Large Renewable Energy Generators: Final Report. Australian Renewable Energy Agency (ARENA) (2022). Available at: https://arena.gov.au/assets/2022/05/harmonic-study-large-renewable-energy-generators-report.pdf (accessed 13 April 2026).

He, J., Li, Y. and Dong, X. (2018) Principles of relay protection in power systems. 5th edn. Beijing: China Electric Power Press.

Kalair, A., Abas, N., Kalair, A.R., Saleem, Z. and Khan, N., 2017. Review of harmonic analysis, modeling and mitigation techniques. Renewable and Sustainable Energy Reviews, 78, pp.1152–1187. Available at: https://doi.org/10.1016/j.rser.2017.04.121

Li, Q., Zhang, S. and Liu, W. (2020) ‘Review on the mechanism and suppression technology of remanent magnetism in power transformer iron core’, Journal of Electrical Engineering Technology, 35(2), pp. 239–252.

Liu, J., Wang, X. and Chen, X. (2021) ‘Simulation study on transformer remanence demagnetization based on MATLAB/Simulink’, Transformer, 58(7), pp. 45–49.

Martínez-Figueroa, G.d.J., Bogarra, S. and Corcoles, F., 2023. Smart Switching in Single-Phase Grid-Connected Photovoltaic Systems to Mitigate Transformer Inrush Currents. Energies, 16(20), 7211. Available at: https://www.mdpi.com/1996-1073/16/20/7211

Wang, Z. and Huang, J. (2019) Power electronics technology. 6th edn. Beijing: Machinery Industry Press.

Wu, H., Wu, J. and Wu, D. (2022) ‘Application of adaptive frequency conversion demagnetization technology in on-site operation and maintenance of large transformers’, High Voltage Electrical Apparatus, 58(3), pp. 187–192.

Wu, J. (2018) Power system simulation technology. Beijing: Beijing Jiaotong University Press.

Wu, M. (2022) Modeling and simulation of transformer electromagnetic characteristics. Beijing: Science Press.

Zhang, S., Yao, C., Zhao, X., Li, J., Liu, X., Yu, L., Ma, J. and Dong, S. (2020) 'Improved flux-controlled VFCV strategy for eliminating and measuring the residual flux of three-phase transformers', IEEE Transactions on Power Delivery, 35, pp. 1237–1248. doi: 10.1109/TPWRD.2019.2937900.

Zhang, X., He, B. and Zhao, H. (2019) ‘Research progress on transformer excitation inrush current recognition and remanence suppression technology’, Power System Automation, 43(11), pp. 182–194.

Zhao, X., Wu, H., Yang, D., Wei, J., Li, Z., Guo, Z. and Zhang, S. (2025) 'Residual magnetism elimination method for large power transformers based on energy storage oscillation', IEEE Transactions on Power Delivery, 40(5), pp. 2759–2768. doi: 10.1109/TPWRD.2025.3589610.

Appendix 1. Source code of the user-defined CVVF S-function controller

```
function [sys,x0,str,ts,simStateCompliance] = text1(t,x,u,flag)

% global u1 k1 k2 ta tb tc flux flux0 flux1 fluxsat fluxsat1 n c1 c2

switch flag,

case 0,
[sys,x0,str,ts,simStateCompliance]=mdlInitializeSizes;

case 1,
sys=mdlDerivatives(t,x,u);

case 2,
sys=mdlUpdate(t,x,u);

case 3,
sys=mdlOutputs(t,x,u);

case 4,
sys=mdlGetTimeOfNextVarHit(t,x,u);

case 9,
sys=mdlTerminate(t,x,u);

otherwise
DAStudio.error('Simulink:blocks:unhandledFlag', num2str(flag));

end
```

```
function [sys,x0,str,ts,simStateCompliance]=mdlInitializeSizes

global u1 k1 k2 ta tb tc flux flux0 flux1 fluxsat n c1 c2
sizes = simsizes;

sizes.NumContStates = 0;
sizes.NumDiscStates = 0;
sizes.NumOutputs = 1;
sizes.NumInputs = 3;
sizes.DirFeedthrough = 1;
sizes.NumSampleTimes = 1; % at least one sample time is needed

sys = simsizes(sizes);

x0 = [];

str = [];

ts = [0.0001 0];

u1=0;

k1=0;

k2=0;

ta=1;

tb=0;
```

```
tc=0;

flux=0;
flux0=0;
flux1=0;
fluxsat=0;
n=0;
c1=0;
c2=0;
simStateCompliance = 'UnknownSimState';

function sys=mdlDerivatives(t,x,u)

sys = [];

function sys=mdlUpdate(t,x,u)

sys = [];

function sys=mdlOutputs(t,x,u)
global u1 k1 k2 ta tb tc flux flux0 flux1 fluxsat fluxsat1 n c1 c2 ;
% double a b c
a=u(1);
b=u(2);
c=u(3);

if k1==0
u1=a;
sys=u1;
```

```
end
if b>=3
k1=1;
u1=-a;
end
if b<=-3
u1=a;
fluxsat1=-0.6*c;
k1=2;
end
if k1==1
sys=u1;
end
if k1==2
sys=u1;
end
if n<14
if (k1==2||k2==2)&& c>=fluxsat1
k1=3;
k2=1;
u1=-a;
fluxsat1=-0.6*fluxsat1;
n=n+1;
end
if k1==3
sys=u1;
end
if k2==1 && c<=fluxsat1
k1=4;
k2=2;
```

```
u1=a;
fluxsat1=-0.6*fluxsat1;
n=n+1;
end
if k1==4
sys=u1;
end
else
sys=0;
end

function sys=mdlGetTimeOfNextVarHit(t,x,u)

sampleTime = 1; % Example, set the next hit to be one second later.
sys = t + sampleTime;
function sys=mdlTerminate(t,x,u)

sys = [];
```